Fourier Expansion for the Electronic Energy Bands in Silicon and Germanium

G. DRESSELHAUS AND M. S. DRESSELHAUS
Lincoln Laboratory, Massachusetts Institute of Technology, Lexington, Massachusetts*
(Received 20 February 1967)

Using a Fourier expansion for the coupled valence and conduction bands in the diamond structure, an effective-mass Hamiltonian valid throughout the Brillouin zone is developed in terms of certain Fourier-expansion coefficients or band parameters which are determined from experimental data. Explicit values for the band parameters are obtained for silicon and germanium, and the resulting energy bands are used to calculate the frequency dependence of the complex dielectric constant. Quantitative agreement is obtained between the calculated and observed dielectric constants. Results are also given for the effective masses for all s and p bands in silicon and germanium at the Γ, L, and X points. The Fourier-expansion technique is computationally simple and rapid, and provides an energy-band model in quantitative agreement with a large number of experimental data.

I. INTRODUCTION

RECENT experimental advances in solid-state spectroscopy[1–3] have made possible a very precise determination of the energy bands in the neighborhood of certain critical points in the joint density of states in solids.[4] Numerous theoretical studies[5–12] of the band structure of solids with the diamond lattice have been carried out, and using these calculations, most of the observed optical structures have been identified with specific interband transitions.[13] In addition to the band-gap determinations by the optical experiments, information is also available on the curvature of some of these bands about their respective critical points. For the semiconductors Si and Ge, accurate cyclotron-resonance measurements have been carried out yielding various effective-mass parameters.[14–17] Experimental information concerning the behavior of the energy bands over the entire Brillouin zone is also available. Reflectivity measurements have been performed over a wide frequency range and have been interpreted to yield the frequency dependence of the complex dielectric constant.[18] Photoemission[19,20] and soft x-ray emission[21,22] studies have also been reported. With the large variety of accurate experimental information that is currently available, it is of interest to determine energy bands throughout the Brillouin zone that are implied by and consistent with these data. Furthermore, it would be valuable for experimentalists to have available to them a theoretical framework, which they could use themselves to refine the energy bands as new optical structures are discovered and new phenomena are explored. To accomplish these aims, a suitable refinement of conventional band calculations would seem appropriate. However, such extensions would involve lengthy numerical computations, and therefore would not readily permit variation of band orderings and the consequent reassignment of optical transitions.

In this paper, a simple effective-mass Hamiltonian is developed for solids that crystallize in the diamond lattice, and this Hamiltonian is valid throughout the whole Brillouin zone. The formulation presented here is sufficiently flexible so that various band orderings can be readily tested and the measured band gaps and effective masses can be simply related to a few band parameters that characterize the Hamiltonian. Using this effective-mass Hamiltonian, the frequency dependence of the dielectric constant is calculated. Detailed applications are made to the two semiconductors silicon and germanium.

Phenomenological band calculations from effective-

* Operated with support from the U. S. Air Force.

[1] B. O. Seraphin and N. Bottka, Phys. Rev. Letters **15**, 104 (1965).
[2] W. E. Engeler, H. Fritzsche, M. Garfinkel, and J. J. Tiemann, Phys. Rev. Letters **14**, 1069 (1965).
[3] G. W. Gobeli and E. O. Kane, Phys. Rev. Letters **15**, 142 (1965).
[4] J. C. Phillips, *Solid State Physics*, edited by F. Seitz and D. Turnbull (Academic Press Inc., New York, 1966), Vol. 18.
[5] J. R. Reitz, *Solid State Physics*, edited by F. Seitz and D. Turnbull (Academic Press Inc., New York, 1955), Vol. 1.
[6] F. Herman, R. L. Kortum, C. D. Kuglin, and R. A. Short, *Quantum Theory of Atoms, Molecules, and the Solid State: A Tribute to J. C. Slater*, edited by Per-Olov Löwdin (Academic Press Inc., New York, 1966).
[7] T. Woodruff, Phys. Rev. **103**, 1159 (1956).
[8] J. C. Phillips and L. Kleinman, Phys. Rev. **116**, 287 (1959); L. Kleinman and J. C. Phillips, *ibid.* **118**, 1152 (1960).
[9] F. Bassani, Nuovo Cimento **13**, 244 (1959).
[10] D. Brust, Phys. Rev. **134**, A1337 (1964).
[11] E. O. Kane, Phys. Rev. **146**, 558 (1966).
[12] M. L. Cohen and T. K. Bergstresser, Phys. Rev. **141**, 789 (1966).
[13] H. Ehrenreich, H. R. Philipp, and J. C. Phillips, Phys. Rev. Letters **8**, 59 (1962).
[14] G. Dresselhaus, A. F. Kip, and C. Kittel, Phys. Rev. **98**, 368 (1955).
[15] B. Lax and J. G. Mavroides, *Solid State Physics*, edited by F. Seitz and D. Turnbull (Academic Press Inc., New York, 1960), Vol. 11.
[16] J. C. Hensel and G. Feher, Phys. Rev. **129**, 1041 (1963).
[17] J. C. Hensel, Solid State Commun. **4**, 231 (1966).
[18] H. R. Philipp and H. Ehrenreich, Phys. Rev. **129**, 1550 (1963).
[19] W. E. Spicer and R. E. Simon, Phys. Rev. Letters **9**, 395 (1962).
[20] F. G. Allen and G. W. Gobeli, Phys. Rev. **144**, 558 (1966).
[21] H. W. B. Skinner, Phil. Trans. Roy. Soc. London **A239**, 95 (1940).
[22] D. H. Tomboulian and D. E. Bedo, Phys. Rev. **104**, 590 (1956).

mass Hamiltonians have been previously developed[23–28] and applied to correlate and interpret various experimental data, but these have generally been limited to fairly small volumes of the Brillouin zone. For example, the $\mathbf{k}\cdot\mathbf{p}$ expansion technique, which is an expansion of the energy about one point, has been successfully applied to various semiconductors.[29] Other interpolation schemes, based on pseudopotential calculations, have been developed to interpret detailed Fermi-surface measurements[30,31] in such metals as Al and Pb. Although these schemes have proven valuable in the analysis of experimental results, the theories are valid over only a limited energy range close to the Fermi level.

The basic ideas underlying the Fourier-expansion technique for electronic energy bands in solids have been previously presented in various forms, but little application of the method has been made to real solids. The Fourier-expansion technique used here is related to a tight-binding calculation for the energy bands,[32] since the *functional form* of the wave-vector-dependent matrix elements is identical in the two treatments. Furthermore, the Fourier-expansion coefficients can be related to integrals involving atomic wave functions. These overlap and transfer integrals are explicitly calculated in the tight-binding treatment, whereas in the Fourier-expansion approach, the expansion coefficients which are related to these overlap and transfer integrals are never calculated from first principles. These coefficients are simply regarded as parameters to be determined from experimental data. Slater and Koster[33] have presented an extension of the tight-binding calculation which gives the most general form for the energy bands, consistent with the lattice symmetry for crystals with cubic symmetry. By actually evaluating the band parameters of these most general energy bands, a rapid convergence of the Fourier expansion is found, thereby indicating that a localized-orbital picture for the electronic energy bands has some validity.

One outstanding application of the tight-binding technique has been made to determine the energy bands in graphite.[34] A Fourier expansion of the graphite energy bands along the vertical edges of the Brillouin zone was carried out by Slonczewski and Weiss,[35] and the expansion coefficients were evaluated by using such detailed experiments as the de Haas–van Alphen effect,[36] the diamagnetic susceptibility,[37] cyclotron resonance,[38–41] and the magnetoreflection.[42] The application of the Fourier-expansion technique to graphite has shown that a vast quantity of experimental data can be correlated and explained by this energy-band model. Since only a few Fourier coefficients need be employed, the rapid convergence of the Fourier series is demonstrated.

Since no such detailed determination of the energy bands from experimental data has yet been successfully attempted for any other solid, the convergence of the Fourier series has never been demonstrated in materials for which the overlap of atomic orbitals is more important. In fact, because of various unsuccessful attempts,[33,43] it has been generally regarded[43,44] that a tight-binding treatment does not provide an adequate representation for the electronic energy bands of such solids. When the tight-binding formalism had been applied previously to these materials, it had been done as an interpolation scheme for energy bands calculated at high-symmetry points.[33,43] In the present paper, it is demonstrated how the Fourier-expansion technique can be used to obtain the electronic energy bands in silicon and germanium from experimental data. Measurements of energy gaps and energy-band curvatures at high-symmetry points in the Brillouin zone, as well as the frequency-dependent dielectric constant, are utilized. Because of its simplicity, this Fourier-expansion method is an attractive computational tool, and has particular merit for systematizing and correlating experimental results.

The presentation of the Fourier-expansion technique in this paper is intended as a working tool for experimentalists in analyzing their data. The theoretical background is presented in Sec. II. Section IIA is devoted to a description of the effective-mass Hamiltonian for the diamond structure. Using this Hamiltonian, expressions for the energy bands and their curvatures in certain high-symmetry directions are given in Sec. IIB. The effect of the spin-orbit interaction in the diamond structure is discussed in Sec. IIC, and, finally, in Sec. IID a calculation of the frequency dependence of the complex dielectric constant is presented. Application of the theoretical background material of Sec. II is made to obtain explicit results for the energy bands and for the frequency-dependent dielectric constant in silicon and germanium in Sec. III.

[23] G. H. Wannier, Phys. Rev. **52**, 191 (1937).
[24] J. M. Luttinger, Phys. Rev. **84**, 814 (1951).
[25] E. N. Adams, II, Phys. Rev. **85**, 41 (1952).
[26] W. Kohn and J. M. Luttinger, Phys. Rev. **97**, 869 (1955).
[27] W. Kohn, Phys. Rev. **115**, 1460 (1959).
[28] L. M. Roth, J. Phys. Chem. Solids, **23**, 433 (1962).
[29] M. Cardona and F. H. Pollak, Phys. Rev. **142**, 530 (1966).
[30] N. W. Ashcroft, Phil. Mag. **8**, 2055 (1963).
[31] J. R. Anderson and A. V. Gold, Phys. Rev. **139**, A1459 (1965).
[32] N. F. Mott and H. Jones, *Theory of the Properties of Metals and Alloys* (Clarendon Press, Oxford, England, 1936).
[33] J. C. Slater and G. F. Koster, Phys. Rev. **94**, 1498 (1954).
[34] F. J. Corbató, Ph.D. thesis, Massachusetts Institute of Technology, 1956 (unpublished).
[35] J. C. Slonczewski and P. R. Weiss, Phys. Rev. **109**, 272 (1958); G. Dresselhaus and M. S. Dresselhaus, Phys. Rev. **140**, A401 (1965).
[36] J. W. McClure, Phys. Rev. **108**, 612 (1957).
[37] J. W. McClure, Phys. Rev. **119**, 606 (1960).
[38] J. Galt, W. Yager, and H. Dail, Jr., Phys. Rev. **103**, 1586 (1956).
[39] P. Nozières, Phys. Rev. **109**, 1510 (1958).
[40] M. Inoue, J. Phys. Soc. Japan **17**, 808 (1962).
[41] S. J. Williamson, M. Surma, H. C. Praddaude, R. A. Patten, and J. K. Furdyna, Solid State Commun. **4**, 37 (1966).
[42] M. S. Dresselhaus and J. G. Mavroides, IBM J. Res. Develop. **8**, 262 (1964).
[43] F. Bassani, Phys. Rev. **108**, 263 (1957).
[44] J. C. Phillips, Phys. Rev. **112**, 685 (1958).

Results are also given for the effective masses for all s and p bands in silicon and germanium at the Γ, L, and X points. The extension of the Fourier expansion to more distant neighbors is treated in Appendix A.

II. THEORETICAL DEVELOPMENT

A. Effective-Mass Hamiltonian for Diamond Lattice

The diamond structure consists of two interpenetrating fcc Bravais lattices which are displaced by $\frac{1}{2}a(1,1,1)$. The Brillouin zone for this structure is the truncated octahedron shown in Fig. 1. There are two atoms/unit cell, and the structure factor vanishes for Bragg reflections from the square face centered about X. This crystal symmetry characterizes the periodic potential seen by the valence and conduction electrons.

Whereas the crystalline potential is periodic in the direct lattice, the electron energy bands $E_n(\mathbf{k})$ can be treated as periodic functions of the reciprocal-lattice vector in the extended-zone scheme. Since $E_n(\mathbf{k})$ is periodic in $\mathbf{k}$, a Fourier expansion

$$E_n(\mathbf{k})=\sum_{\mathbf{d}} \epsilon_n(\mathbf{d})e^{i\mathbf{k}\cdot\mathbf{d}} \tag{1}$$

can be made in terms of the vectors $\mathbf{d}$ of the direct lattice. The Fourier coefficients $\epsilon_n(\mathbf{d})$ constitute the band parameters which characterize the energy bands. The crystal symmetry of the diamond lattice greatly restricts the number of independent band parameters, and if the Fourier expansion is rapidly convergent, the energy bands can be completely specified in terms of only a few band parameters. In fact, rapid convergence of the series is required for practical applications of the Fourier-expansion technique.

The symmetry operations and associated character tables for the diamond structure have been enumerated by Herring.[45] The symmetry operations include various screw and glide operations which are point-group operations of the fcc lattice followed by translations by a nonprimitive lattice vector. The additional degeneracies associated with the *two interpenetrating* fcc lattices are easily handled in terms of the symmetry of the electronic wave functions.

In order to demonstrate these symmetries, it is convenient to choose tight-binding wave functions as basis functions. However, it should be emphasized that except for these symmetry considerations, no explicit use is made of tight-binding functions in constructing an effective-mass Hamiltonian for the diamond lattice. The tight-binding bonding and antibonding wave functions $\Psi_+(\mathbf{k})$ and $\Psi_-(\mathbf{k})$ for the diamond structure are written in terms of linear combinations of the atomic orbitals $\psi(\mathbf{r}_i)$ and $\psi(\mathbf{r}_i+\tau)$ centered about atoms of each sublattice:

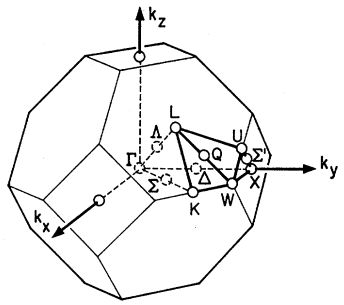

FIG. 1. Brillouin zone for the diamond lattice in which some of the high-symmetry points and axes are indicated.

$$\Psi_\pm(\mathbf{k})=\frac{1}{(2N)^{1/2}}\sum_{\text{fcc}} e^{i\mathbf{k}\cdot\mathbf{r}_i}[\psi(\mathbf{r}_i)\pm\psi(\mathbf{r}_i+\tau)e^{i\mathbf{k}\cdot\tau}], \tag{2}$$

where $\tau=\frac{1}{2}a(1,1,1)$ is the displacement of these two sublattices and $\mathbf{r}_i$ represents the direct fcc lattice vectors: $\mathbf{r}_0=a(0,0,0)$, $\mathbf{r}_1=a(1,1,0)$, $\mathbf{r}_2=a(2,0,0)$, etc. The internal symmetries of this crystal structure yield relationships between the wave functions at $\mathbf{k}$ and at the displaced wave vectors $\mathbf{k}'=\mathbf{k}+(\pi/a)(2,0,0)$ and $\mathbf{k}''=\mathbf{k}+(\pi/a)(1,1,1)$, given by

$$\begin{aligned}&\Psi_\pm(\mathbf{k}+(\pi/a)(2,0,0))=\Psi_\mp(\mathbf{k}),\\ &\Psi_\pm(\mathbf{k}+(\pi/a)(1,1,1))=\frac{(1\mp i)}{2}\Psi_+(\mathbf{k})+\frac{(1\pm i)}{2}\Psi_-(\mathbf{k}).\end{aligned} \tag{3}$$

Using these crystal symmetries, an effective-mass Hamiltonian for the diamond lattice has been developed that is valid throughout the entire Brillouin zone.[46] Eight coupled energy bands are explicitly considered which arise from states having symmetries Γ_1, $\Gamma_{25'}$, $\Gamma_{2'}$, and Γ_{15} at $\mathbf{k}=0$ (the Γ point). These symmetry types include all the symmetries encountered in coupling s and p bonding and antibonding states. Although this formulation does not explicitly include all the symmetry types for other bands (such as d bands), the effect of such bands is implicitly contained in the actual evaluation of the band parameters that enter into the effective-mass Hamiltonian. Since these band parameters are evaluated directly from experimental observations, contributions to the actual magnitudes of the parameters are included for all bands, regardless of their symmetries. By carrying out a $\mathbf{k}\cdot\mathbf{p}$ expansion of the effective-mass Hamiltonian about high-symmetry points, the relative importance of the various bands, which are not included explicitly, is found using the experimentally determined values of the band parameters.

The effective-mass Hamiltonian for n coupled bands

[45] C. Herring, J. Franklin Inst. **233**, 525 (1942). The extension to double group representations required in treating the spin-orbit interaction is given by R. J. Elliott [Phys. Rev. **96**, 280 (1954)].

[46] G. Dresselhaus (to be published): A preliminary account of this work is given in G. Dresselhaus and M. S. Dresselhaus, *The Optical Properties of Solids*, edited by J. Tauc (Academic Press Inc., New York, 1966), p. 198.

is written[46] as an $(n\times n)$ matrix of the form

$$\mathcal{H}(\mathbf{k})=\begin{pmatrix}\mathcal{H}^{++}(\mathbf{k}) & \mathcal{H}^{+-}(\mathbf{k})\\ \mathcal{H}^{-+}(\mathbf{k}) & \mathcal{H}^{--}(\mathbf{k})\end{pmatrix}, \tag{4}$$

where each of the square matrices $\mathcal{H}^{++}$, $\mathcal{H}^{+-}$, $\mathcal{H}^{-+}$, $\mathcal{H}^{--}$ is of dimensionality $n/2$. The symmetry relations given by Eq. (3) require that n be even; that is, the bands are required to occur in pairs. For example, when the symmetry types Γ_1 or Γ_{15} are considered, the related symmetry types $\Gamma_{2'}$ and $\Gamma_{25'}$, respectively, must also be included in order to satisfy Eq. (3). The symmetry relations of Eq. (3), in fact, relate the matrices of Eq. (4) in the following way:

$$\begin{aligned}&\mathcal{H}^{++}(\mathbf{k}+(\pi/a)(2,0,0))=\mathcal{H}^{--}(\mathbf{k})\\ &\mathcal{H}^{++}(\mathbf{k}+(\pi/a)(1,1,1))=\tfrac{1}{2}[\mathcal{H}^{++}(\mathbf{k})+\mathcal{H}^{--}(\mathbf{k})]\\ &\qquad\qquad+\tfrac{1}{2}i[\mathcal{H}^{+-}(\mathbf{k})-\mathcal{H}^{-+}(\mathbf{k})].\end{aligned} \tag{5}$$

The matrices $\mathcal{H}^{++}$ and $\mathcal{H}^{--}$ transform as Γ_1, whereas $\mathcal{H}^{+-}$ and $\mathcal{H}^{-+}$ transform as $\Gamma_{2'}$. In addition, invariance under time-inversion symmetry requires that the matrix elements of the $(n\times n)$ Hamiltonian are related by

$$\mathcal{H}_{ij}{}^{*}(-\mathbf{k})=\mathcal{H}_{ij}(\mathbf{k}). \tag{6}$$

Using these symmetry conditions, the Hamiltonian can be written in terms of four Hermitian matrices $h_0(\mathbf{k})$, $h_1(\mathbf{k})$, $g_0(\mathbf{k})$, and $g_1(\mathbf{k})$ as

$$\mathcal{H}(\mathbf{k})=\begin{pmatrix}h_0(\mathbf{k})+h_1(\mathbf{k}) & g_0(\mathbf{k})-ig_1(\mathbf{k})\\ g_0(\mathbf{k})+ig_1(\mathbf{k}) & h_0(\mathbf{k})-h_1(\mathbf{k})\end{pmatrix}, \tag{7}$$

in which $h_0(\mathbf{k})$ is the Hamiltonian for the fcc lattice. Application of the symmetry relations of Eqs. (5) and (6) to Eq. (7) yields the symmetry properties

$$\begin{aligned}&h_0(\mathbf{k}+(\pi/a)(2,0,0))=h_0(\mathbf{k}),\\ &h_0(\mathbf{k}+(\pi/a)(1,1,1))=h_0(\mathbf{k}),\\ &h_1(\mathbf{k}+(\pi/a)(2,0,0))=-h_1(\mathbf{k}),\\ &h_1(\mathbf{k}+(\pi/a)(1,1,1))=g_1(\mathbf{k}).\end{aligned} \tag{8}$$

The off-diagonal matrices of Eq. (7), $g_1(\mathbf{k})$ and $g_0(\mathbf{k})$, are, respectively, antisymmetric and symmetric under time-reversal symmetry. The symmetry relations of Eq. (8) are generally valid and characterize the diamond lattice whether a particular crystal is to be described by 2 coupled bands (e.g., only s bands), by 6 bands (only p bands), by 8 bands (s-p bands), by 18 bands (s-p-d bands), or by the spin-orbit split bands ($p_{1/2}$,$p_{3/2}$). These symmetry relations guarantee that the energy bands exhibit all the necessary band degeneracies at symmetry points and along symmetry axes.

In the case of silicon and germanium, the effective-mass Hamiltonian is written as an (8×8) matrix, and other bands that are of lesser importance near the Fermi level are included implicitly in the evaluation of the band parameters. With $n=8$, the (4×4) matrix $h_0(\mathbf{k})$ representing the Hamiltonian for the related fcc lattice is written as

$$\begin{aligned}h_0(\mathbf{k})=&[\gamma_{0,1}-4\gamma_{1,1}+\gamma_{2,1}C(2,\mathbf{k};\Gamma_1)]S(s,\Gamma_1)\\ &+[\gamma_{0,2}-4\gamma_{1,2}+\gamma_{2,2}C(2,\mathbf{k};\Gamma_1)]S(p,\Gamma_1)\\ &+\gamma_{2,5}\mathbf{C}^{*}(2,\mathbf{k};\Gamma_{12})\cdot\mathbf{S}(p,\Gamma_{12})\\ &+\gamma_{2,3}\mathbf{C}(2,\mathbf{k};\Gamma_{25'})\cdot\mathbf{S}(p,\Gamma_{25'})\\ &+\gamma_{2,4}\mathbf{C}(2,\mathbf{k};\Gamma_{15})\cdot\mathbf{S}(sp,\Gamma_{15})+\cdots.\end{aligned} \tag{9}$$

In this equation, the Fourier-expansion coefficients $\gamma_{\alpha,\beta}$ are the band parameters for the energy bands, the index α denotes the αth nearest-neighbor distance $\mathbf{d}_\alpha$ of the direct lattice $\alpha=0, 1, 2, \cdots$, and the index β enumerates the band parameters that can occur for a given value of α, namely $\beta=1, 2, \cdots, \beta_{\max}$. The Fourier expansion in Eq. (9) is written explicitly up to and including terms at the next-neighbor separation or $\alpha=2$. In order to compare the band parameters $\gamma_{\alpha,\beta}$ with equivalent band parameters that have appeared in the work of Slater and Koster[33] and Dresselhaus,[46] Table I is included. Because of time-reversal symmetry, the Hamiltonian can always be written in a form such that the band parameters $\gamma_{\alpha,\beta}$ are real c numbers, independent of crystal momentum $\mathbf{k}$. In this way, all the $\mathbf{k}$ dependence in the effective-mass Hamiltonian is contained in the symmetrized Fourier-functions $C(\alpha,\mathbf{k};\Gamma_\beta)$, where Γ_β denotes one of the β symmetry types which occurs for the αth nearest-neighbor distance. A listing

TABLE I. Notation for band parameters.

This paper	D[a]	$S-K$[b]
$\gamma_{0,1}$	$24\alpha[(000),\Gamma_1;\Gamma_1\leftrightarrow\Gamma_1]$	$E_{s,s}(000)+4E_{s,s}(\frac{1}{2}\frac{1}{2}\frac{1}{2})$
	$+24\alpha[(\frac{1}{2}\frac{1}{2}\frac{1}{2}),\Gamma_1;\Gamma_1\leftrightarrow\Gamma_1]$	$+12E_{s,s}(110)$
	$+24\alpha[(110),\Gamma_1;\Gamma_1\leftrightarrow\Gamma_1]$	
$\gamma_{0,2}$	$24\alpha[(000),\Gamma_{15}\leftrightarrow\Gamma_{15}]$	$E_{x,x}(000)+4E_{x,x}(\frac{1}{2}\frac{1}{2}\frac{1}{2})$
	$+24\alpha[(\frac{1}{2}\frac{1}{2}\frac{1}{2}),\Gamma_1;\Gamma_{15}\leftrightarrow\Gamma_{15}]$	$+8E_{x,x}(110)+4E_{x,x}(011)$
	$+24\alpha[(110),\Gamma_1;\Gamma_{15}\leftrightarrow\Gamma_{15}]$	
$\gamma_{1,1}$	$6\alpha[(\frac{1}{2}\frac{1}{2}\frac{1}{2}),\Gamma_1;\Gamma_1\leftrightarrow\Gamma_1]$	$E_{s,s}(\frac{1}{2}\frac{1}{2}\frac{1}{2})$
$\gamma_{1,2}$	$6\alpha[(\frac{1}{2}\frac{1}{2}\frac{1}{2}),\Gamma_1;\Gamma_{15}\leftrightarrow\Gamma_{15}]$	$E_{x,x}(\frac{1}{2}\frac{1}{2}\frac{1}{2})$
$\gamma_{1,3}$	$6\alpha[(\frac{1}{2}\frac{1}{2}\frac{1}{2}),\Gamma_{25'};\Gamma_{15}\leftrightarrow\Gamma_{15}]$	$E_{x,y}(\frac{1}{2}\frac{1}{2}\frac{1}{2})$
$\gamma_{1,4}$	$6\alpha[(\frac{1}{2}\frac{1}{2}\frac{1}{2}),\Gamma_{15};\Gamma_1\leftrightarrow\Gamma_{15}]$	$E_{s,x}(\frac{1}{2}\frac{1}{2}\frac{1}{2})$
$\gamma_{2,1}$	$4\alpha[(110),\Gamma_1;\Gamma_1\leftrightarrow\Gamma_1]$	$2E_{s,s}(110)$
$\gamma_{2,2}$	$4\alpha[(110),\Gamma_1;\Gamma_{15}\leftrightarrow\Gamma_{15}]$	$\frac{2}{3}[E_{x,x}(011)+2E_{x,x}(110)]$
$\gamma_{2,3}$	$4\alpha[(110),\Gamma_{25'};\Gamma_{15}\leftrightarrow\Gamma_{15}]$	$2E_{x,y}(110)$
$\gamma_{2,4}$	$4\alpha[(110),\Gamma_{15};\Gamma_1\leftrightarrow\Gamma_{15}]$	$2E_{s,x}(110)$
$\gamma_{2,5}$	$4\alpha[(110),\Gamma_{12};\Gamma_{15}\leftrightarrow\Gamma_{15}]$	$\frac{2}{3}[E_{x,x}(011)-E_{x,x}(110)]$
$\gamma_{2,6}$	$4\alpha[(110),\Gamma_{25'};\Gamma_1\leftrightarrow\Gamma_{25'}]$	$2E_{s,x}(011)$[c]
$\gamma_{2,7}$	$4\alpha[(110),\Gamma_{25};\Gamma_{15}\leftrightarrow\Gamma_{25'}]$	$-2E_{x,y}(011)$[c]

[a] See Ref. 46.

[b] The Slater-Koster Hamiltonian (Ref. 33) $\mathcal{H}_{S.K.}$ is related to the Hamiltonian used in this paper by a unitary transformation.

$$\mathcal{H}_{S.K.}=\begin{pmatrix}h_0+g_0 & h_1+ig_1\\ h_1-ig_1 & h_0-g_0\end{pmatrix}.$$

[c] There is a misprint in Table V of Ref. 33. The correct entries are

$$(s|x)_{11}=-4E_{s,x}(011)\sin\zeta\sin\eta+4iE_{s,x}(110)\sin\xi(\cos\eta+\cos\zeta),$$
$$(x|y)_{11}=-4E_{x,y}(110)\sin\xi\sin\eta-4iE_{x,y}(011)\sin\zeta(\cos\xi-\cos\eta),$$

and $(y|z)_{11}$ is obtained from $(x|y)_{11}$ by a cyclic permutation of ξ, η, ζ plus a complex conjugation.

TABLE II. Symmetrized Fourier functions for a diamond lattice.[a]

$a(000)$	$C(0,\mathbf{k};\Gamma_1)=$	1
$\frac{1}{2}a(1,1,1)$	$C(1,\mathbf{k};\Gamma_1)=$	$-4+\cos\frac{1}{2}a(k_x+k_y+k_z)+\cos\frac{1}{2}a(k_x-k_y-k_z)+\cos\frac{1}{2}a(-k_x+k_y-k_z)+\cos\frac{1}{2}a(-k_x-k_y+k_z)$
	$C(1,\mathbf{k};\Gamma_{2'})=$	$\sin\frac{1}{2}a(k_x+k_y+k_z)+\sin\frac{1}{2}a(k_x-k_y-k_z)+\sin\frac{1}{2}a(-k_x+k_y-k_z)+\sin\frac{1}{2}a(-k_x-k_y+k_z)$
	$C_x(1,\mathbf{k};\Gamma_{15})=$	$\sin\frac{1}{2}a(k_x+k_y+k_z)+\sin\frac{1}{2}a(k_x-k_y-k_z)-\sin\frac{1}{2}a(-k_x+k_y-k_z)-\sin\frac{1}{2}a(-k_x-k_y+k_z)$
	$C_x(1,\mathbf{k};\Gamma_{25'})=$	$\cos\frac{1}{2}a(k_x+k_y+k_z)+\cos\frac{1}{2}a(k_x-k_y-k_z)-\cos\frac{1}{2}a(-k_x+k_y-k_z)-\cos\frac{1}{2}a(-k_x-k_y+k_z)$
$a(1,1,0)$	$C(2,\mathbf{k};\Gamma_1)=$	$-6+\cos a(k_y+k_z)+\cos a(k_y-k_z)+\cos a(k_z+k_x)+\cos a(k_z-k_x)+\cos a(k_x+k_y)+\cos a(k_x-k_y)$
	$C_1(2,\mathbf{k};\Gamma_{12})=$	$[\cos a(k_y+k_z)+\cos a(k_y-k_z)]+\omega[\cos a(k_z+k_x)+\cos a(k_z-k_x)]+\omega^2[\cos a(k_x+k_y)+\cos a(k_x-k_y)]$
	$C_x(2,\mathbf{k};\Gamma_{15})=$	$\sin a(k_x+k_y)+\sin a(k_x-k_y)+\sin a(k_x+k_z)+\sin a(k_x-k_z)$
	$C_x(2,\mathbf{k};\Gamma_{25'})=$	$\cos a(k_y+k_z)-\cos a(k_y-k_z)$
	$C_x(2,\mathbf{k};\Gamma_{25})=$	$\sin a(k_x+k_y)+\sin a(k_x-k_y)-\sin a(k_x+k_z)-\sin a(k_x-k_z)$

[a] A cyclic permutation of k_x, k_y, k_z gives the functions $C_y(n,\mathbf{k};\Gamma_i)$ and $C_z(n,\mathbf{k};\Gamma_i)$ whereas $C_2(n,\mathbf{k};\Gamma_{12})=[C_1(n,\mathbf{k};\Gamma_{12})]^*$; $\mathbf{C}(n,\mathbf{k};\Gamma_{12})=(C_1(n,\mathbf{k};\Gamma_{12}), C_2(n;\mathbf{k},\Gamma_{12}))$ and $\omega=\exp(2\pi i/3)$.

of the symmetrized Fourier functions for the diamond lattice ($\alpha=0,1,2$) is given in Table II. The $C(\alpha,\mathbf{k};\Gamma_\beta)$ functions are one-dimensional vectors for symmetries Γ_1 and $\Gamma_{2'}$, two-dimensional vectors for symmetry Γ_{12}, and three-dimensional vectors for symmetries Γ_{15}, Γ_{25}, and $\Gamma_{25'}$. Since no commutivity has been assumed for the $\mathbf{k}$ vectors, the $C(\alpha,\mathbf{k};\Gamma_\beta)$ functions can be treated as operators, as must be done in the presence of an external magnetic field.

The remaining factors that enter into Eq. (9) are the (4×4) basis matrices $S(i,\Gamma_\beta)$. The index i is a band label and the Γ_β denote the symmetry types. A list of the $S(i,\Gamma_\beta)$ matrices that occur in the effective-mass Hamiltonian for silicon and germanium is given in Table III. For symmetry Γ_1, only one basis matrix is involved, while for Γ_{12} symmetry, two (4×4) matrices are required [i.e., $\mathbf{S}(p,\Gamma_{12})$ is a two-dimensional vector of (4×4) matrices]. Similarly, for Γ_{15}, $\Gamma_{15'}$, and $\Gamma_{25'}$ symmetries, three related basis matrices occur so that, for example, $\mathbf{S}(p,\Gamma_{25'})$ denotes three (4×4) matrices. The dot-product notation, which occurs in Eq. (9) and subsequently, represents a summation over appropriate components of the symmetrized Fourier-function vectors with the corresponding basis matrix. For example, for the Γ_{15}, Γ_{25}, and $\Gamma_{25'}$ symmetries $\mathbf{C}\cdot\mathbf{S}=C_xS_x+C_yS_y+C_zS_z$, while for Γ_{12} symmetry $\mathbf{C}^*\cdot\mathbf{S}=C_1^*S_1+C_1S_2$. See Tables II and III for explicit expressions for $\mathbf{C}$ and $\mathbf{S}$.

Whereas the (4×4) matrix $h_0(\mathbf{k})$ of Eq. (7) is even under the translation $\mathbf{k}\rightarrow\mathbf{k}+(\pi/a)(2,0,0)$, the (4×4) matrix $h_1(\mathbf{k})$ is odd under this translation, and

$$h_1(\mathbf{k})=\gamma_{1,1}[4+C(1,\mathbf{k};\Gamma_1)]S(s,\Gamma_1)+\gamma_{1,2}[4+C(1,\mathbf{k};\Gamma_1)]\times S(p,\Gamma_1)+\gamma_{1,3}\mathbf{C}(1,\mathbf{k};\Gamma_{25'})\cdot\mathbf{S}(p,\Gamma_{25'})+\gamma_{1,4}\mathbf{C}(1,\mathbf{k};\Gamma_{15})\cdot\mathbf{S}(sp,\Gamma_{15})+\cdots, \quad (10)$$

where the band parameters $\gamma_{\alpha,\beta}$, the symmetrized Fourier functions $C(\alpha,\mathbf{k};\Gamma_\beta)$, and the (4×4) basis matrices $S(i,\Gamma_\beta)$ are listed respectively in Tables I–III. Here again, the Fourier expansion is terminated at next-nearest-neighbor terms $\alpha=2$.

The off-diagonal matrices in the effective-mass Hamiltonian of Eq. (7) are either symmetric or antisymmetric under time inversion. The symmetric matrix $g_0(\mathbf{k})$ is written as

$$g_0(\mathbf{k})=\gamma_{2,6}\mathbf{C}(2,\mathbf{k};\Gamma_{25'})\cdot\mathbf{S}(sp,\Gamma_{25'})+\gamma_{2,7}\mathbf{C}(2,\mathbf{k};\Gamma_{25})\cdot\mathbf{S}(p,\Gamma_{15'})+\cdots, \quad (11)$$

and the antisymmetric matrix $g_1(\mathbf{k})$ is obtained from

TABLE III. Basis matrices.[a]

$$S_x(sp,\Gamma_{15})=\begin{pmatrix}0&i&0&0\\-i&&&\\0&&\mathcal{O}&\\0&&&\end{pmatrix}$$

$$S_y(sp,\Gamma_{15})=\begin{pmatrix}0&0&i&0\\0&&&\\-i&&\mathcal{O}&\\0&&&\end{pmatrix}$$

$$S_z(sp,\Gamma_{15})=\begin{pmatrix}0&0&0&i\\0&&&\\0&&\mathcal{O}&\\-i&&&\end{pmatrix}$$

$$S_x(sp,\Gamma_{25'})=\begin{pmatrix}0&1&0&0\\1&&&\\0&&\mathcal{O}&\\0&&&\end{pmatrix}$$

$$S_y(sp,\Gamma_{25'})=\begin{pmatrix}0&0&1&0\\0&&&\\1&&\mathcal{O}&\\0&&&\end{pmatrix}$$

$$S_z(sp,\Gamma_{25'})=\begin{pmatrix}0&0&0&1\\0&&&\\0&&\mathcal{O}&\\1&&&\end{pmatrix}$$

$$S(s,\Gamma_1)=\begin{pmatrix}1&0&0&0\\0&&&\\0&&\mathcal{O}&\\0&&&\end{pmatrix}$$

$$S(p,\Gamma_1)=\begin{pmatrix}0&0&0&0\\0&1&0&0\\0&0&1&0\\0&0&0&1\end{pmatrix}$$

[a] The other pertinent basis matrices are related to those in the table by the expressions:

$$S_x(p,\Gamma_{25'})=S_y(sp,\Gamma_{15})S_z(sp,\Gamma_{15})+S_z(sp,\Gamma_{15})S_y(sp,\Gamma_{15}),$$
$$S_x(p,\Gamma_{15'})=i\{S_y(sp,\Gamma_{15})S_z(sp,\Gamma_{15})-S_z(sp,\Gamma_{15})S_y(sp,\Gamma_{15})\},$$ and

$S_y(p,\Gamma_i)$ and $S_z(p,\Gamma_i)$ are obtained by cyclic permutations of x, y, z. Further,

$$S_1(p,\Gamma_{12})=[S_x(sp,\Gamma_{15})]^2+\omega[S_y(sp,\Gamma_{15})]^2+\omega^2[S_z(sp,\Gamma_{15})]^2,$$

$S_2(p,\Gamma_{12})$ is the Hermitian conjugate of $S_1(p,\Gamma_{12})$, $\mathcal{O}$ is a (3×3) null matrix, and $\omega=\exp(2\pi i/3)$.

$h_1(\mathbf{k})$ by a translation $\mathbf{k}\rightarrow\mathbf{k}+(\pi/a)(1,1,1)$ according to Eq. (8):

$$g_1(\mathbf{k})=\gamma_{1,1}C(1,\mathbf{k};\Gamma_{2'})S(s,\Gamma_1)+\gamma_{1,2}C(1,\mathbf{k};\Gamma_{2'})S(p,\Gamma_1)+\gamma_{1,3}\mathbf{C}(1,\mathbf{k};\Gamma_{15})\cdot\mathbf{S}(p,\Gamma_{25'})-\gamma_{1,4}\mathbf{C}(1,\mathbf{k};\Gamma_{25'})\cdot\mathbf{S}(sp,\Gamma_{15})+\cdots. \quad (12)$$

The effective-mass Hamiltonian presented in Eqs. (7)–(12) and Tables I–III can be applied to write dispersion relations $E_n(\mathbf{k})$ for the energy bands for materials which crystallize in the diamond structure. By terminating the Fourier expansion with terms involving next-nearest-neighbor interactions ($\alpha=2$), these energy bands are described by 13 band parameters, where 2 are associated with distance $\mathbf{d}_0=a(0,0,0)$, 4 are associated with $\mathbf{d}_1=\frac{1}{2}a(1,1,1)$, and 7 with $\mathbf{d}_2=a(1,1,0)$. In Appendix A, the terms in the effective-mass Hamiltonian arising from interactions at third- and fourth-nearest-neighbor distances are presented. Since, for example, the distance $|\mathbf{d}_3|$ is not much larger than $|\mathbf{d}_2|$, it would be expected that some higher-order Fourier terms could provide quantitative refinement of the energy bands discussed in this paper.

The energy bands for the various materials which crystallize in the diamond structure are described by the same effective-mass Hamiltonian but differ in the actual values of the band parameters and the relative importance of the spin-orbit interaction discussed in Sec. IIC. That is, the explicit values of the band parameters determine whether the solid is a semiconductor, a semimetal, or a metal. Furthermore, this Hamiltonian can also be applied, with slight modification because of the lack of inversion symmetry, to describe the energy bands of various III-V compounds which crystallize in the zinc-blende lattice, e.g., InSb. This application is discussed in Ref. 46.

B. Energy Bands along High-Symmetry Directions

The (8×8) effective-mass Hamiltonian simplifies considerably along high-symmetry axes and at high-symmetry points in the Brillouin zone. Since experimental information is used to determine the band parameters, and, furthermore, since many experiments are particularly sensitive to the energy bands at high-symmetry points, explicit formulas are given in this section for the energy bands at the high-symmetry points Γ, X, K, and L and along the axes Δ, Σ, and Λ (see Fig. 1).

TABLE IV. Connectivity relations.

Δ axis	
$\Gamma_1\rightarrow\Delta_1$	
$\Gamma_{15}\rightarrow\Delta_1,\Delta_5$	
$\Gamma_{2'}\rightarrow\Delta_{2'}$	
$\Gamma_{25'}\rightarrow\Delta_{2'},\Delta_5$	
$\Delta_1(\Gamma)\rightarrow\Delta_1(X)\rightarrow\Delta_{2'}(\Gamma)\rightarrow\Delta_{2'}(X)\rightarrow\Delta_1(\Gamma)$	
$\Delta_5(\Gamma)\rightarrow\Delta_5(X)\rightarrow\Delta_5(\Gamma)$	
Λ axis	
$\Gamma_1\rightarrow\Lambda_1$	$L_1,L_{2'}\rightarrow\Lambda_1$
$\Gamma_{15}\rightarrow\Lambda_1,\Lambda_3$	
$\Gamma_{2'}\rightarrow\Lambda_1$	$L_3,L_{3'}\rightarrow\Lambda_3$
$\Gamma_{25'}\rightarrow\Lambda_1,\Lambda_3$	
Σ axis	
$\Gamma_1\rightarrow\Sigma_1$	
$\Gamma_{15}\rightarrow\Sigma_1,\Sigma_3,\Sigma_4$	
$\Gamma_{2'}\rightarrow\Sigma_3$	
$\Gamma_{25'}\rightarrow\Sigma_1,\Sigma_2,\Sigma_3$	

1. Δ Axis

Along the Γ-X or Δ axis, the crystal-momentum vector is $(k_x,k_y,k_z)=(\kappa,0,0)$ and the effective-mass Hamiltonian can be factored. That this factorization occurs can be understood by elementary group-theoretical considerations.[45] By using the connectivity relations given in Table IV it is seen that along Γ-X the one-dimensional representation Δ_1 occurs twice, the one-dimensional representation $\Delta_{2'}$ occurs twice, and the two-dimensional representation Δ_5 also occurs twice. The degree of the secular equation is governed by the number of times an irreducible representation occurs. Thus, the (8×8) Hamiltonian is expected to break up into two (2×2) blocks yielding nondegenerate eigenvalues $E^{\pm}(\Delta_1)$ and $E^{\pm}(\Delta_{2'})$ and one (4×4) block with two double degenerate eigenvalues $E^{\pm}(\Delta_5)$.

By direct substitution of $\mathbf{k}=(\kappa,0,0)$ into Eqs. (7)–(12) and by Tables II and III, the nonvanishing matrix elements h_{ij} of the effective-mass Hamiltonian along Δ are found to be

$$\begin{aligned}
h_{11}(\kappa)&=\gamma_{0,1}-4\gamma_{1,1}(1-\cos\tfrac{1}{2}a\kappa)-4\gamma_{2,1}(1-\cos a\kappa),\\
h_{22}(\kappa)&=\gamma_{0,2}-4\gamma_{1,2}(1-\cos\tfrac{1}{2}a\kappa)\\
&\quad-4(\gamma_{2,2}-\gamma_{2,5})(1-\cos a\kappa),\\
h_{33}(\kappa)&=h_{44}(\kappa)=\gamma_{0,2}-4\gamma_{1,2}(1-\cos\tfrac{1}{2}a\kappa)\\
&\quad-4(\gamma_{2,2}+\tfrac{1}{2}\gamma_{2,5})(1-\cos a\kappa),\\
h_{12}(\kappa)&=4i(\gamma_{1,4}\sin\tfrac{1}{2}a\kappa+\gamma_{2,4}\sin a\kappa),\\
h_{38}(\kappa)&=h_{47}(\kappa)=-4i\gamma_{1,3}\sin\tfrac{1}{2}a\kappa.
\end{aligned} \quad (13)$$

The remaining nonvanishing matrix elements are related to those given in Eq. (13) by the symmetry conditions derived from Eq. (8):

$$h_{i'j'}(\kappa)=h_{ij}(\kappa+2\pi/a), \quad (14)$$

for $i'=i+4$, $j'=j+4$, and $i,j\leqslant 4$, and by the Hermitian character of the Hamiltonian $h_{ji}(\kappa)=h_{ij}{}^*(\kappa)$. Under the symmetry operation $\kappa\rightarrow\kappa+2\pi/a$ of Eq. (14), $\cos\frac{1}{2}a\kappa\rightarrow-\cos\frac{1}{2}a\kappa$, while $\cos a\kappa$ is invariant. In these equations, the definition of the distance a in the direct lattice, places atoms at $a(0,0,0)$, $\frac{1}{2}a(1,1,1)$, $a(1,1,0)$, etc., where $a=2.71$ Å in silicon and 2.83 Å in germanium.

The dispersion relations along the Δ axis are found by solution of the secular equation implied by the Hamiltonian of Eq. (13). The nondegenerate roots are easily found to be

$$E^{\pm}(\Delta_1)=\tfrac{1}{2}[h_{11}+h_{22}\pm((h_{11}-h_{22})^2+4|h_{12}|^2)^{1/2}],$$

$$E^{\pm}(\Delta_{2'})=\tfrac{1}{2}[h_{55}+h_{66}\pm((h_{55}-h_{66})^2+4|h_{56}|^2)^{1/2}],$$

while the doubly degenerate set is given by

$$E^{\pm}(\Delta_5)=\tfrac{1}{2}[h_{33}+h_{77}\pm((h_{33}-h_{77})^2+4|h_{38}|^2)^{1/2}]. \quad (15)$$

In particular, at the Γ point (0,0,0), the expressions for the nondegenerate energy bands become

$$E(\Gamma_1)=\gamma_{0,1},$$
$$E(\Gamma_{2'})=\gamma_{0,1}-8\gamma_{1,1},$$

and the triply degenerate levels are

$$\begin{aligned} E(\Gamma_{15})&=\gamma_{0,2},\\ E(\Gamma_{25'})&=\gamma_{0,2}-8\gamma_{1,2}\equiv 0, \end{aligned} \tag{16}$$

in which the zero of energy is fixed at $E(\Gamma_{25'})$, the top of the valence band.

Likewise, at point X, where $a\kappa=\pi$, four doubly degenerate levels result,

$$\begin{aligned} E^{\pm}(X_4)&=\gamma_{0,2}-4\gamma_{1,2}-8\gamma_{2,2}-4\gamma_{2,5}\pm 4\gamma_{1,3},\\ E^{\pm}(X_1)&=\tfrac{1}{2}[\chi_{11}+\chi_{22}\pm((\chi_{11}-\chi_{22})^2+4|\chi_{12}|^2)^{1/2}], \end{aligned} \tag{17}$$

in which

$$\begin{aligned} \chi_{11}&=\gamma_{0,1}-4\gamma_{1,1}-8\gamma_{2,1},\\ \chi_{22}&=\gamma_{0,2}-4\gamma_{1,2}-8\gamma_{2,2}+8\gamma_{2,5},\\ \chi_{12}&=4i\gamma_{1,4}. \end{aligned} \tag{18}$$

These band degeneracies at points Γ and X along the Δ axis are seen in the energy bands for silicon shown in Fig. 2. It should be emphasized that the Δ_1 and $\Delta_{2'}$ levels have no greater symmetry at the X point than at an arbitrary point along the Δ axis. That is, in an extended-zone scheme, points along the Δ axis obey the connectivity relation $\Gamma\rightarrow X\rightarrow\Gamma$, shown in Table IV. Therefore, the Δ_1 and $\Delta_{2'}$, levels interchange their symmetry at X and become $\Delta_{2'}$ and Δ_1 levels, respectively. Thus, since the Δ_1 and $\Delta_{2'}$, levels can have nonzero slopes at the X point, the X point does not generally represent a critical point in the joint density of states for interband transitions to the $E^{\pm}(X_1)$ bands.

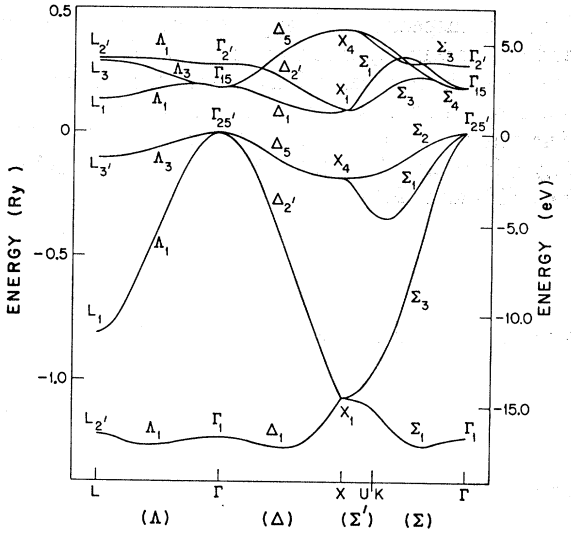

FIG. 2. Energy versus dimensionless wave vector for a few high-symmetry directions in silicon. Spin-orbit interaction has been neglected.

On the other hand, the double degeneracy of the Δ_5 levels automatically guarantees that the $E^{\pm}(\Delta_5)$ levels approach X with zero slope. However, when the effect of spin-orbit interaction is considered, the degeneracy of the $E^{\pm}(\Delta_5)$ levels is lifted and none of the energy bands need approach X with zero slope. These symmetry considerations are treated in greater detail by Herring.[45]

2. Σ Axis

Along the Σ axis, $\Gamma\rightarrow K\rightarrow X$, the substitution $\mathbf{k}=(\kappa,\kappa,0)$ is made. In this case, the nonvanishing matrix elements $h_{ij}(\kappa)$ of the effective-mass Hamiltonian are

$$\begin{aligned} h_{11}(\kappa)&=\gamma_{0,1}-2\gamma_{1,1}(1-\cos a\kappa)+\gamma_{2,1}(-5+4\cos a\kappa+\cos 2a\kappa),\\ h_{22}(\kappa)&=h_{33}(\kappa)=\gamma_{0,2}-2\gamma_{1,2}(1-\cos a\kappa)+\gamma_{2,2}(-5+4\cos a\kappa+\cos 2a\kappa)+\gamma_{2,5}(2\cos a\kappa-1-\cos 2a\kappa),\\ h_{44}(\kappa)&=\gamma_{0,2}-2\gamma_{1,2}(1-\cos a\kappa)+\gamma_{2,2}(-5+4\cos a\kappa+\cos 2a\kappa)-2\gamma_{2,5}(2\cos a\kappa-1-\cos 2a\kappa),\\ h_{12}(\kappa)&=h_{13}(\kappa)=i[2\gamma_{1,4}\sin a\kappa+\gamma_{2,4}(\sin 2a\kappa+2\sin a\kappa)],\\ h_{23}(\kappa)&=-2\gamma_{1,3}(1-\cos a\kappa)-\gamma_{2,3}(1-\cos 2a\kappa),\\ h_{18}(\kappa)&=2\gamma_{1,4}(1-\cos a\kappa)-\gamma_{2,6}(1-\cos 2a\kappa),\\ h_{28}(\kappa)&=h_{38}(\kappa)=i[-2\gamma_{1,3}\sin a\kappa+\gamma_{2,7}(\sin 2a\kappa-2\sin a\kappa)]. \end{aligned} \tag{19}$$

Using the symmetry relations of Eq. (8) and the Hermitian property of the matrices $h_0(\mathbf{k})$, $h_1(\mathbf{k})$, $g_0(\mathbf{k})$, and $g_1(\mathbf{k})$ in Eq. (7), the other nonvanishing matrix elements of the effective-mass Hamiltonian are related to those of Eq. (19) by

$$\begin{aligned} h_{55}(\kappa)&=h_{11}(\kappa)-4\gamma_{1,1}(1+\cos a\kappa),\\ h_{jj}(\kappa)&=h_{ii}(\kappa)-4\gamma_{1,2}(1+\cos a\kappa)\qquad i=2,3,4;\ j=i+4,\\ h_{56}(\kappa)&=h_{57}(\kappa)=h_{12}(\kappa)-4\gamma_{1,4}\sin a\kappa,\\ h_{67}(\kappa)&=h_{23}(\kappa)+4\gamma_{1,3}(1-\cos a\kappa),\\ h_{45}(\kappa)&=h_{18}(\kappa)-4\gamma_{1,4}(1-\cos a\kappa),\\ h_{46}(\kappa)&=h_{47}(\kappa)=h_{28}(\kappa)-2i\gamma_{2,7}(\sin 2a\kappa-2\sin a\kappa),\\ h_{ji}(\kappa)&=h_{ij}{}^{*}(\kappa). \end{aligned} \tag{20}$$

By direct inspection, it is apparent that the (8×8) effective-mass Hamiltonian along the Σ axis, given in Eqs. (19) and (20), breaks up into two uncoupled (4×4) blocks. However, from the connectivity relations of Table IV, it is seen that the representations Σ_2 and Σ_4 each occur once, while Σ_1 and Σ_3 both occur three times. Therefore, there must exist a unitary transformation which transforms each of the (4×4) blocks into a (1×1) and a (3×3) block. The unitary transformation that accomplishes this factorization is the one that transforms the basis vectors (x,y,z) into $(2^{-1/2}(x+y),\ 2^{-1/2}(x-y),\ z)$. The resulting Σ_2 and Σ_4 energy levels are related to the matrix elements of Eqs. (19) and (20) by

$$\begin{aligned} E(\Sigma_2)&=h_{66}(\kappa)-h_{67}(\kappa)\,,\\ E(\Sigma_4)&=h_{22}(\kappa)-h_{23}(\kappa)\,, \end{aligned} \tag{21}$$

while the dispersion relations for the $E(\Sigma_1)$ and $E(\Sigma_3)$ bands are found by solution of the secular equations

$$\begin{vmatrix} h_{11}(\kappa)-E(\Sigma_1) & \sqrt{2}h_{12}(\kappa) & h_{18}(\kappa) \\ -\sqrt{2}h_{12}(\kappa) & h_{22}(\kappa)+h_{23}(\kappa)-E(\Sigma_1) & \sqrt{2}h_{28}(\kappa) \\ h_{18}(\kappa) & -\sqrt{2}h_{28}(\kappa) & h_{88}(\kappa)-E(\Sigma_1) \end{vmatrix}=0\,, \tag{22}$$

and

$$\begin{vmatrix} h_{44}(\kappa)-E(\Sigma_3) & h_{45}(\kappa) & \sqrt{2}h_{46}(\kappa) \\ h_{45}(\kappa) & h_{55}(\kappa)-E(\Sigma_3) & \sqrt{2}h_{56}(\kappa) \\ -\sqrt{2}h_{46}(\kappa) & -\sqrt{2}h_{56}(\kappa) & h_{66}(\kappa)+h_{67}(\kappa)-E(\Sigma_3) \end{vmatrix}=0\,. \tag{23}$$

The solutions to Eqs. (21)–(23) at the Γ point ($\kappa=0$) reduce properly to the dispersion relations given by Eq. (16) and obey the connectivity relations of Table IV. Since the energy bands at the K point, $a\kappa=3\pi/4$, are not especially simple, no explicit expressions need be written here. Furthermore, the K point has no higher symmetry than an arbitrary point along the Σ axis. Therefore, the K point need not be a critical point and the energy bands along the Σ axis will, in general, have nonzero slope at K.

On the other hand, the energy levels at point X are simpler and are given by the expressions of Eqs. (17) and (18), which were derived by approaching the X point along the Δ axis. However, when the X point is approached along the Σ axis, substitution of $a\kappa=\pi$ into Eq. (21) results in

$$E^-(X_4)=E(\Sigma_2)\,|_{\kappa=\pi/a}=\tfrac{1}{2}\gamma_{0,2}-8\gamma_{2,2}-4\gamma_{2,5}-4\gamma_{1,3} \tag{24}$$

for the $E(\Sigma_2)$ level, and

$$E^+(X_4)=E(\Sigma_4)\,|_{\kappa=\pi/a}=E(\Sigma_2)\,|_{\kappa=\pi/a}+8\gamma_{1,3} \tag{25}$$

for the $E(\Sigma_4)$ level. The connectivity relations $\Gamma_{25'}\rightarrow\Sigma_2\rightarrow X_4$ and $\Gamma_{15}\rightarrow\Sigma_4\rightarrow X_4$ do, in fact, determine the sign of $\gamma_{1,3}$. Since at the Γ point, $E(\Sigma_2)$ becomes one of the degenerate-valence bands $E(\Gamma_{25'})$, it is necessary that $E^-(X_4)<0$, if the crystal is to be an insulator or semiconductor. Similarly, since $E(\Sigma_4)$ becomes one of the degenerate-conduction bands $E(\Gamma_{15})$, it is necessary that $E^+(X_4)>0$. Thus, in order both to satisfy the connectivity relations and require that the crystal be insulating or semiconducting, it follows from Eq. (25) that

$$\gamma_{1,3}>0\,. \tag{26}$$

By restricting $\gamma_{1,3}$ to positive values, the actual determination of the band parameters in silicon and germanium is greatly simplified.

Whereas the energy bands of Fig. 2 along the Σ axis exhibit various slopes at the K point, all of the energy levels come into X with zero slope. This would make X appear to have especially high symmetry, but in fact the energy levels along directions parallel to the Σ axis also come into the appropriate point on Δ axis with zero slope.

3. Λ *Axis*

Along the Λ axis, the appropriate substitution is $\mathbf{k}=(\kappa,\kappa,\kappa)$. The connectivity relations of Table IV show that the two-dimensional representation Λ_3 is contained twice and the one-dimensional representation Λ_1 occurs four times. Therefore, the (8×8) Hamiltonian must factor into two (4×4) blocks, one of which has two sets of doubly degenerate roots, while the other has, in general, four distinct roots. The unitary transformation, which decouples the (8×8) matrix into two (4×4) blocks, is that transformation which sends the basis functions (x,y,z) into the linear combinations $3^{-1/2}(x+y+z,\ x+\omega y+\omega^2 z,\ x+\omega^2 y+\omega z)$ where $\omega=e^{2\pi i/3}$. After this unitary transformation has been

performed, the nonvanishing matrix elements of the resulting Hamiltonian are

$$\begin{aligned}
h_{11}(\kappa)&=\gamma_{0,1}+\gamma_{1,1}(-4+\cos\tfrac{3}{2}a\kappa+3\cos\tfrac{1}{2}a\kappa)-3\gamma_{2,1}(1-\cos 2a\kappa),\\
h_{22}(\kappa)&=\gamma_{0,2}+\gamma_{1,2}(-4+\cos\tfrac{3}{2}a\kappa+3\cos\tfrac{1}{2}a\kappa)+2\gamma_{1,3}(\cos\tfrac{3}{2}a\kappa-\cos\tfrac{1}{2}a\kappa)-(3\gamma_{2,2}+2\gamma_{2,3})(1-\cos 2a\kappa),\\
h_{33}(\kappa)&=h_{44}(\kappa)=h_{22}(\kappa)-3\gamma_{1,3}(\cos\tfrac{3}{2}a\kappa-\cos\tfrac{1}{2}a\kappa)+3\gamma_{2,3}(1-\cos 2a\kappa),\\
h_{12}(\kappa)&=i\sqrt{3}[\gamma_{1,4}(\sin\tfrac{3}{2}a\kappa+\sin\tfrac{1}{2}a\kappa)+2\gamma_{2,4}\sin 2a\kappa],\\
h_{15}(\kappa)&=-i\gamma_{1,1}(\sin\tfrac{3}{2}a\kappa-3\sin\tfrac{1}{2}a\kappa),\\
h_{26}(\kappa)&=-i[\gamma_{1,2}(\sin\tfrac{3}{2}a\kappa-3\sin\tfrac{1}{2}a\kappa)+2\gamma_{1,3}(\sin\tfrac{3}{2}a\kappa+\sin\tfrac{1}{2}a\kappa)],\\
h_{16}(\kappa)&=-\sqrt{3}[\gamma_{1,4}(\cos\tfrac{3}{2}a\kappa-\cos\tfrac{1}{2}a\kappa)+\gamma_{2,6}(1-\cos 2a\kappa)],
\end{aligned}\tag{27}$$

and the remaining nonvanishing matrix elements are related to these by

$$\begin{aligned}
h_{55}(\kappa)&=h_{11}(\kappa)-2\gamma_{1,1}(\cos\tfrac{3}{2}a\kappa+3\cos\tfrac{1}{2}a\kappa),\\
h_{66}(\kappa)&=h_{22}(\kappa)-2\gamma_{1,2}(\cos\tfrac{3}{2}a\kappa+3\cos\tfrac{1}{2}a\kappa)-4\gamma_{1,3}(\cos\tfrac{3}{2}a\kappa-\cos\tfrac{1}{2}a\kappa),\\
h_{77}(\kappa)&=h_{88}(\kappa)=h_{33}(\kappa)-2\gamma_{1,2}(\cos\tfrac{3}{2}a\kappa+3\cos\tfrac{1}{2}a\kappa)+2\gamma_{1,3}(\cos\tfrac{3}{2}a\kappa-\cos\tfrac{1}{2}a\kappa),\\
h_{56}(\kappa)&=h_{12}(\kappa)-2i\sqrt{3}\gamma_{1,4}(\sin\tfrac{3}{2}a\kappa+\sin\tfrac{1}{2}a\kappa),\\
h_{37}(\kappa)&=h_{48}(\kappa)=h_{26}(\kappa)+3i\gamma_{1,3}(\sin\tfrac{3}{2}a\kappa+\sin\tfrac{1}{2}a\kappa),\\
h_{25}(\kappa)&=h_{16}(\kappa)+2\sqrt{3}\gamma_{1,4}(\cos\tfrac{3}{2}a\kappa-\cos\tfrac{1}{2}a\kappa),\\
h_{ji}(\kappa)&=h_{ij}{}^{*}(\kappa).
\end{aligned}\tag{28}$$

The doubly degenerate $E^{\pm}(\Lambda_3)$ levels are given by

$$E^{\pm}(\Lambda_3)=\tfrac{1}{2}[h_{33}(\kappa)+h_{77}(\kappa)\pm\{(h_{33}(\kappa)-h_{77}(\kappa))^2+4|h_{37}(\kappa)|^2\}^{1/2}],\tag{29}$$

while the $E(\Lambda_1)$ levels are found by solution of the secular equation

$$\begin{vmatrix}
h_{11}-E(\Lambda_1) & h_{12} & h_{15} & h_{16}\\
h_{12}{}^{*} & h_{22}-E(\Lambda_1) & h_{25} & h_{26}\\
h_{15}{}^{*} & h_{25}{}^{*} & h_{55}-E(\Lambda_1) & h_{56}\\
h_{16}{}^{*} & h_{26}{}^{*} & h_{56}{}^{*} & h_{66}-E(\Lambda_1)
\end{vmatrix}=0,\tag{30}$$

where the matrix elements are defined in Eqs. (27) and (28). The eigenvalues of Eqs. (29) and (30) reduce properly to the Γ-point energies in accordance with the connectivity relations of Table IV.

The energy eigenvalues at the L point are obtained by substitution of $a\kappa=\frac{1}{2}\pi$ into Eqs. (29) and (30). Because of the additional symmetry at the L point, a unitary transformation can be applied to transform the (4×4) matrix at the L point into two (2×2) blocks. The resulting eigenvalues for the $E^{\pm}(L_1)$ and $E^{\pm}(L_{2'})$ levels are

$$\begin{aligned}
E^{\pm}(L_i)=\tfrac{1}{2}[&A(L_i)+B(L_i)\\
&\pm\{[A(L_i)-B(L_i)]^2+4|C(L_i)|^2\}^{1/2}],
\end{aligned}\tag{31}$$

where

$$\begin{aligned}
A(L_1)&=\gamma_{0,1}-6\gamma_{1,1}-6\gamma_{2,1},\\
B(L_1)&=\gamma_{0,2}-2\gamma_{1,2}-4\gamma_{1,3}-6\gamma_{2,2}-4\gamma_{2,3},\\
C(L_1)&=-2\sqrt{3}(\gamma_{1,4}+\gamma_{2,6}),
\end{aligned}\tag{32a}$$

and

$$\begin{aligned}
A(L_{2'})&=A(L_1)+4\gamma_{1,1},\\
B(L_{2'})&=B(L_1)-4\gamma_{1,2}+8\gamma_{1,3},\\
C(L_{2'})&=C(L_1)+4\sqrt{3}\gamma_{1,4}.
\end{aligned}\tag{32b}$$

Similarly, simple expressions are found for the two doubly degenerate levels at the L point:

$$E^{\pm}(L_3)=\gamma_{0,2}-4\gamma_{1,2}-6\gamma_{2,2}+2\gamma_{2,3}\pm 2(\gamma_{1,2}+\gamma_{1,3}).\tag{33}$$

In the literature, it has been customary to denote $E^{+}(L_3)$ by $E(L_3)$, and $E^{-}(L_3)$ by $E(L_{3'})$; and this notation is also used in this paper.

These formulas for the energy levels at the L point are particularly useful in the band-parameter determination because the formulas are reasonably simple and, secondly, because considerable experimental information is available with regard to these energy levels and their curvatures. The L point is a critical point in the joint density of states since all the energy levels approach L with zero slope, regardless of the direction of approach to L.

4. *Energy-Band Curvatures at* Γ

Extensive experimental information is available not only for energy band gaps at high-symmetry points in the Brillouin zone, but also for band curvatures (or effective masses) at these symmetry points. By carrying out a Taylor-series expansion of the effective-mass Hamiltonian of Eq. (7), expressions for the band

curvatures are obtained. Although such an expansion can be carried out about any point in the Brillouin zone, only at very-high-symmetry points are the expressions simple enough to write down explicitly. In particular, the expressions about $\mathbf{k}=0$ are both simple and useful, because of the accurate effective-mass data available for the energy bands about the Γ point. In this section, expansion formulas for $\mathbf{k}=0$ are presented. On the other hand, the expansion formulas about the L point and about a point on the Δ axis are sufficiently complicated so that, in practice, numerical methods are found to be more convenient in calculating band curvatures for these points.

A Taylor expansion for the effective-mass Hamiltonian of Eq. (7) is made to terms in k^2 for the diagonal entries and to terms linear in k for the off-diagonal terms. Use of second-order perturbation theory for the off-diagonal terms yields the expansions for the nondegenerate energy bands:

$$E(\Gamma_1;\mathbf{k})=\gamma_{0,1}+(ak)^2 \times\left[-\tfrac{1}{2}\gamma_{1,1}-2\gamma_{2,1}+\frac{(2\gamma_{1,4}+4\gamma_{2,4})^2}{E(\Gamma_1)-E(\Gamma_{15})}\right], \quad (34a)$$

$$E(\Gamma_{2'};\mathbf{k})=\gamma_{0,1}-8\gamma_{1,1}+(ak)^2 \times\left\{\tfrac{1}{2}\gamma_{1,1}-2\gamma_{2,1}+\frac{(-2\gamma_{1,4}+4\gamma_{2,4})^2}{E(\Gamma_{2'})-E(\Gamma_{25'})}\right\}, \quad (34b)$$

in which $E(\Gamma_i)$ is the energy eigenvalue at Γ, given by Eq. (16). It is of interest to observe that the band curvatures for these nondegenerate levels are more sensitive to the high-Fourier coefficients than are the energy levels themselves. Furthermore, the same result is also found for the energy-band curvatures at the other high-symmetry points in the Brillouin zone. For this reason, by terminating the Fourier expansion with terms for $\alpha\leq 2$, the energy levels are more accurately represented than the corresponding band curvatures. Therefore, greater weight is given to the position of the energy levels than to the band curvatures in carrying out the actual band-parameter evaluation.

The expansion for the threefold degenerate levels $E(\Gamma_{15})$ and $E(\Gamma_{25'})$ is carried out by solving a determinantal equation for the three strongly coupled bands which is of the form

$$\begin{vmatrix} L\xi^2+M(\eta^2+\zeta^2)-\lambda & N\xi\eta & N\xi\zeta \\ N\xi\eta & L\eta^2+M(\zeta^2+\xi^2)-\lambda & N\eta\zeta \\ N\xi\zeta & N\eta\zeta & L\zeta^2+M(\xi^2+\eta^2)-\lambda \end{vmatrix}=0, \quad (35a)$$

where

$$\lambda=E(\Gamma_i;\mathbf{k})-E(\Gamma_i), \quad (35b)$$

and

$$(\xi,\eta,\zeta)=a(k_x,k_y,k_z). \quad (35c)$$

The determinantal Eq. (35) is identical in form to the well-known $\mathbf{k}\cdot\mathbf{p}$ result,[14] except for a few small differences in notation. The quantities L, M, and N which appear in Eq. (35) have the dimensions of energy and are related to the L', M', and N' of the literature[14] by

$$(L,M)=a^{-2}(L',M')+\hbar^2/2m_0a^2, \quad N=a^{-2}N', \quad (36)$$

so that the free-electron contribution to the band curvature is already included in L and M. The quantities L, M, and N for the $E(\Gamma_{15})$ levels are related to the band parameters $\gamma_{i,j}$ by

$$L(\Gamma_{15})=-\tfrac{1}{2}\gamma_{1,2}-2\gamma_{2,2}+2\gamma_{2,5}+\frac{(2\gamma_{1,4}+4\gamma_{2,4})^2}{E(\Gamma_{15})-E(\Gamma_1)}, \quad (37)$$

$$M(\Gamma_{15})=-\tfrac{1}{2}\gamma_{1,2}-2\gamma_{2,2}-\gamma_{2,5}+\frac{4(\gamma_{1,3})^2}{E(\Gamma_{15})-E(\Gamma_{25'})}, \quad (38)$$

$$Q(\Gamma_{15})=L(\Gamma_{15})+M(\Gamma_{15})-N(\Gamma_{15}) =-\gamma_{1,2}-4\gamma_{2,2}+\gamma_{2,5}+\gamma_{1,3}+2\gamma_{2,3}, \quad (39)$$

and for the $E(\Gamma_{25'})$ levels by

$$L(\Gamma_{25'})=\tfrac{1}{2}\gamma_{1,2}-2\gamma_{2,2}+2\gamma_{2,5}+\frac{(-2\gamma_{1,4}+4\gamma_{2,4})^2}{E(\Gamma_{25'})-E(\Gamma_{2'})}, \quad (40)$$

$$M(\Gamma_{25'})=\tfrac{1}{2}\gamma_{1,2}-2\gamma_{2,2}-\gamma_{2,5}+\frac{4(\gamma_{1,3})^2}{E(\Gamma_{25'})-E(\Gamma_{15})}, \quad (41)$$

$$Q(\Gamma_{25'})=L(\Gamma_{25'})+M(\Gamma_{25'})-N(\Gamma_{25'}) =\gamma_{1,2}-4\gamma_{2,2}+\gamma_{2,5}-\gamma_{1,3}+2\gamma_{2,3}, \quad (42)$$

in which the $E(\Gamma_i)$ are defined in Eq. (16). Experimental data are available for the quantities $L(\Gamma_{25'})$, $M(\Gamma_{25'})$, and $Q(\Gamma_{25'})$ in silicon and germanium from analysis of the cyclotron-resonance measurements of holes in the degenerate valence band $E(\Gamma_{25'})$. No experimental information is yet available for the corresponding quantities for the conduction band $E(\Gamma_{15})$. However, these quantities can be calculated according to Eqs. (37)–(39), once the band parameters have been evaluated.

The dispersion relations [Eqs. (34)–(35)] for the energy bands in the neighborhood of the Γ point are very similar in form to that given by the $\mathbf{k}\cdot\mathbf{p}$ perturbation theory.[14,47] For example, the $\mathbf{k}\cdot\mathbf{p}$ result for non-

[47] E. I. Blount, *Solid State Physics*, edited by F. Seitz and D. Turnbull (Academic Press Inc., New York, 1962), Vol. 13, p. 305.

degenerate bands is

$$E(\Gamma_1,\mathbf{k})=E(\Gamma_1)+\frac{\hbar^2k^2}{2m_0}+\hbar^2k^2\sum_l\frac{|(\alpha|v_x|\delta_{xl})|^2}{E(\Gamma_1)-E_l(\Gamma_{15})}, \quad (43)$$

in which the summation is over the integer l, which labels bands with Γ_{15} symmetry, and the notation for the matrix elements is that used in Ref. 14. A comparison between Eqs. (34a) and (43) emphasizes the characteristic features of the two expansion procedures. First of all, the velocity matrix element in the Fourier-expansion approach is directly evaluated in terms of specific band parameters by taking derivatives of the effective-mass Hamiltonian according to the prescription[47,48]

$$\mathbf{v}(\mathbf{k})=\frac{1}{\hbar}\frac{\partial}{\partial\mathbf{k}}\mathcal{H}(\mathbf{k}). \quad (44a)$$

This expression, which is based upon the effective-mass approximation, emphasizes the relation between band curvatures and the $\mathbf{k}$-dependent velocity matrix elements which determine the intensity of an interband optical transition. Such identifications of matrix elements and effective-mass Hamiltonians have been made in treating the infrared absorption in silicon and germanium,[49] cyclotron resonance in graphite,[40] and interband transitions in bismuth.[50] The pertinent assumption of the effective-mass approximation is that in the presence of an electromagnetic field, the vector $\mathbf{k}$ in the effective-mass Hamiltonian is replaced by the operator $-i\nabla-(e/\hbar c)\mathbf{A}$. The resulting effective-mass Hamiltonian can then be expanded as

$$\mathcal{H}\left(-i\nabla-\frac{e}{\hbar c}\mathbf{A}\right)=\mathcal{H}(-i\nabla)-\frac{e}{2m_0c}[\mathbf{A}\cdot\mathbf{p}(-i\nabla)+\mathbf{p}(-i\nabla)\cdot\mathbf{A}]+\cdots, \quad (44b)$$

in which the perturbation Hamiltonian associated with the electromagnetic fields is written in the customary way. With this identification, the operator $\mathbf{p}(-i\nabla)=m_0\mathbf{v}(-i\nabla)$ is evaluated according to Eq. (44a). The utility of this approach is that the k dependence for both the diagonal and off-diagonal matrix elements of $\mathbf{p}$ is calculated, and the selection rules for optical transitions are determined directly from the effective-mass Hamiltonian. Therefore, nonvanishing matrix elements for $\mathbf{p}$ can only occur between those bands explicitly coupled in $\mathcal{H}(\mathbf{k})$.

With this interpretation of the matrix elements of $\mathbf{p}=m_0\mathbf{v}$ in the Fourier-expansion approach, only one term enters the sum of Eq. (34a), whereas the summation in Eq. (43) is over all Γ_{15} states. However, the most important term in the sum is that term which directly corresponds to the one and only Fourier-expansion term. It might therefore seem that the Fourier-expansion technique neglects these other bands, but this is not actually the case. The effect of the bands that are not explicitly treated is, nevertheless, implicitly included both in the actual evaluation of the Fourier-expansion coefficients from experimental measurements and in the contribution to the dispersion relation from diagonal terms in the effective-mass Hamiltonian.

The treatment of these diagonal terms represents the other striking difference between Eqs. (34a) and (43), and is closely connected with the contrasting origins of the two techniques. On one hand, the $\mathbf{k}\cdot\mathbf{p}$ expansion is based on a free-electron model, and the unperturbed mass is the free-electron mass m_0. On the other hand, the Fourier-expansion technique is based on a tight-binding model, and, therefore, the unperturbed mass m_{TB} is simply related to certain Fourier-expansion parameters (or overlap integrals), i.e., $(\hbar^2/2m_{\mathrm{TB}})=a^2[-\frac{1}{2}\gamma_{1,1}-2\gamma_{2,1}]$. The inequality between the tight-binding mass m_{TB} and the free-electron mass can be used to account for the neglect of bands which are not treated explicitly in the Fourier-expansion approach. To put this another way, the effect of more distant bands is treated in the $\mathbf{k}\cdot\mathbf{p}$ approach by increasing the number of bands or the dimensionality of the effective-mass Hamiltonian, whereas in the Fourier-expansion approach, it is only necessary to add higher Fourier coefficients, *without increasing the dimensionality of the Hamiltonian*. Since the dimensionality of the Hamiltonian is fixed at the minimal number of bands required by symmetry to yield a semiconductor, the Fourier-expansion approach offers practical computational advantages.

C. Spin-Orbit Interaction

In the previous section, dispersion relations were given for the energy bands at various high-symmetry points and axes. At these points and axes, band degeneracies commonly occur. Many of these band degeneracies are lifted by the spin-orbit interaction. Therefore, whenever the energy associated with the spin-orbit interaction is large enough to be comparable with other band separations, no accurate band-parameter determination can be carried out without including this interaction.

The effect of the spin-orbit interaction can easily be treated within the Fourier-expansion formulation. The spin-orbit term in the effective-mass Hamiltonian is Fourier expanded and the Fourier-expansion coefficients become spin-orbit band parameters, which are to be determined from experiment. If the spin-orbit interaction is small compared with other band separations (e.g., s-p band splittings), then perturbation theory suggests that only a few Fourier coefficients are required to adequately represent the spin-orbit term,

[48] G. H. Wannier, Rev. Mod. Phys. **34**, 645 (1952).
[49] A. H. Kahn, Phys. Rev. **97**, 1647 (1955).
[50] P. A. Wolff, J. Phys. Chem. Solids **25**, 1057 (1964).

In this section only one spin-orbit band parameter is used to characterize the spin-orbit splitting everywhere in the Brillouin zone.

The effective-mass Hamiltonian for the diamond lattice including spin-orbit interaction is developed by considering first the matrix $\mathcal{H}^{++}(\mathbf{k})$ of Eq. (4) for coupled s and p bands (i.e., Γ_1 and Γ_{15} bands). This (4×4) matrix $\mathcal{H}^{++}(\mathbf{k})$ is written in Eq. (4) in a (s,p_x,p_y,p_z) representation. Spin is incorporated into the problem by introducing eight basis functions $(s\uparrow,p_x\uparrow,p_y\uparrow,p_z\uparrow;\ s\downarrow,p_x\downarrow,p_y\downarrow,p_z\downarrow)$. Since $\mathcal{H}^{++}(\mathbf{k})$ does not depend on spin, a related (8×8) matrix $\mathcal{H}_0{}^{++}(\mathbf{k})$ can be written as

$$\mathcal{H}_0{}^{++}(\mathbf{k})=\begin{pmatrix}\mathcal{H}^{++}(\mathbf{k}) & \mathcal{O}\\ \mathcal{O} & \mathcal{H}^{++}(\mathbf{k})\end{pmatrix}, \tag{45}$$

where $\mathcal{O}$ is a (4×4) zero block. A unitary transformation is then performed upon $\mathcal{H}_0{}^{++}(\mathbf{k})$ to change the representation into a $(s_{1/2},p_{1/2},p_{3/2})$ representation in which the spin-orbit interaction $\mathcal{H}_{s\text{-}o}$ is diagonal and the transformed matrix is written as

$$\tilde{\mathcal{H}}_0{}^{++}(\mathbf{k})=U\mathcal{H}_0{}^{++}(\mathbf{k})U^{+}. \tag{46}$$

The matrix U which accomplishes this basis transformation is given in Table V. In a similar way, the same unitary transformation is then applied to construct the other (8×8) blocks, $\tilde{\mathcal{H}}_0{}^{--}(\mathbf{k})$, $\tilde{\mathcal{H}}_0{}^{+-}(\mathbf{k})$, $\tilde{\mathcal{H}}_0{}^{-+}(\mathbf{k})$, of the effective-mass Hamiltonian in a representation appropriate to the spin problem, with

$$\tilde{\mathcal{H}}_0(\mathbf{k})=\begin{pmatrix}\tilde{\mathcal{H}}_0{}^{++}(\mathbf{k}) & \tilde{\mathcal{H}}_0{}^{+-}(\mathbf{k})\\ \tilde{\mathcal{H}}_0{}^{-+}(\mathbf{k}) & \tilde{\mathcal{H}}_0{}^{--}(\mathbf{k})\end{pmatrix}. \tag{47}$$

The 16 eigenvalues of this Hamiltonian break up into 8 doubly degenerate pairs; and each pair coincides with one of the eigenvalues of $\mathcal{H}(\mathbf{k})$ in Eq. (7).

The eigenvalues are, however, modified by the inclusion of spin-orbit interaction, and the effect is most significant at those points in the Brillouin zone where band degeneracies are present. It is convenient to write the spin-orbit interaction Hamiltonian as

$$\mathcal{H}_{s\text{-}o}(\mathbf{k})=\begin{pmatrix}\mathcal{H}_{s\text{-}o}{}^{++}(\mathbf{k}) & \mathcal{H}_{s\text{-}o}{}^{+-}(\mathbf{k})\\ \mathcal{H}_{s\text{-}o}{}^{-+}(\mathbf{k}) & \mathcal{H}_{s\text{-}o}{}^{--}(\mathbf{k})\end{pmatrix}, \tag{48}$$

where use has been made of the symmetry properties of the diamond structure given in Eq. (8). Each of the four (8×8) blocks in Eq. (48) is then Fourier expanded. Since for many applications (e.g., silicon and germanium) the spin-orbit energies are sufficiently small, it is necessary to retain only the leading or constant term in the Fourier expansion. Then $\mathcal{H}_{s\text{-}o}$ is independent of $\mathbf{k}$ and is constant throughout the whole Brillouin zone. This $\mathbf{k}$-independent $\mathcal{H}_{s\text{-}o}$ nevertheless allows the spin-orbit splitting of the actual energy levels in the crystal to be $\mathbf{k}$ dependent. In the case of the $\mathbf{k}$-independent $\mathcal{H}_{s\text{-}o}$, the matrices $\mathcal{H}_{s\text{-}o}{}^{++}$ and $\mathcal{H}_{s\text{-}o}{}^{--}$ only have

TABLE V. Coupling coefficients for the p bands.[a]

	$p_x\uparrow$	$p_y\uparrow$	$p_z\uparrow$	$p_x\downarrow$	$p_y\downarrow$	$p_z\downarrow$
$p_{1/2}{}^{(1/2)}$	0	0	$-\frac{i}{\sqrt{3}}$	$-\frac{i}{\sqrt{3}}$	$\frac{1}{\sqrt{3}}$	0
$p_{1/2}{}^{(-1/2)}$	$-\frac{i}{\sqrt{3}}$	$-\frac{1}{\sqrt{3}}$	0	0	0	$\frac{i}{\sqrt{3}}$
$p_{3/2}{}^{(3/2)}$	$-\frac{i}{\sqrt{2}}$	$\frac{1}{\sqrt{2}}$	0	0	0	0
$p_{3/2}{}^{(1/2)}$	0	0	$i(\frac{2}{3})^{1/2}$	0	$-\frac{i}{\sqrt{6}}$	$\frac{1}{(\sqrt{6}$
$p_{3/2}{}^{(-1/2)}$	$-\frac{i}{\sqrt{6}}$	$\frac{1}{\sqrt{6}}$	0	0	0	$(\frac{2}{3}^{1/2}$
$p_{3/2}{}^{(-3/2)}$	0	0	0	$\frac{i}{\sqrt{2}}$	$\frac{1}{\sqrt{2}}$	0

[a] In this table, the unitary transformation U is defined by

$$U\begin{bmatrix}s\uparrow\\ p_x\uparrow\\ p_y\uparrow\\ p_z\uparrow\\ s\downarrow\\ p_x\downarrow\\ p_y\downarrow\\ p_z\downarrow\end{bmatrix}=\begin{bmatrix}s\uparrow\\ s\downarrow\\ p_{1/2}{}^{(1/2)}\\ p_{1/2}{}^{(-1/2)}\\ p_{3/2}{}^{(3/2)}\\ p_{3/2}{}^{(1/2)}\\ p_{3/2}{}^{(-1/2)}\\ p_{3/2}{}^{(-3/2)}\end{bmatrix}$$

diagonal entries depending on the spin-orbit band parameter Δ

$$(\mathcal{H}_{s\text{-}o}{}^{++})_{ij}=(\mathcal{H}_{s\text{-}o}{}^{--})_{ij}=x_{ii}\delta_{ij},$$

with the diagonal terms given by

$$\begin{aligned}&x_{11}=x_{22}=0,\\ &x_{33}=x_{44}=-\tfrac{2}{3}\Delta,\\ &x_{55}=x_{66}=x_{77}=x_{88}=\tfrac{1}{3}\Delta,\end{aligned} \tag{49}$$

and the off-diagonal matrices are (8×8) zero blocks

$$\mathcal{H}_{s\text{-}o}{}^{+-}=\mathcal{H}_{s\text{-}o}{}^{-+}=\mathcal{O}. \tag{50}$$

The effective-mass Hamiltonian including spin-orbit interaction $\mathcal{H}_{tot}$ is then written as

$$\mathcal{H}_{tot}(\mathbf{k})=\tilde{\mathcal{H}}_0(\mathbf{k})+\mathcal{H}_{s\text{-}o}, \tag{51}$$

in terms of the matrices defined in Eqs. (47) and (48).

The effect of the spin-orbit interaction is to lift various band degeneracies, although without a magnetic field the necessary twofold Kramers degeneracy remains. At the Γ point, the 16 energy eigenvalues of $\tilde{\mathcal{H}}_0(\mathbf{k})$ break up into two doubly degenerate s levels and two sixfold degenerate p levels. The spin-orbit interaction splits each of these p levels into a twofold $p_{1/2}$ level and a fourfold $p_{3/2}$ level. If only the leading term in the Fourier expansion of $\mathcal{H}_{s\text{-}o}$ is retained, as in Eqs. (49) and (50), then the splittings in the valence and conduction p bands at Γ are both equal to Δ, with the $p_{3/2}$ levels moving up by $\frac{1}{3}\Delta$ and the $p_{1/2}$ levels moving down by $\frac{2}{3}\Delta$; thus, the center of gravity of the p-band multiplet is retained in the presence of the

spin-orbit interaction. Although there is no theoretical reason why the spin-orbit interaction at Γ should be describable in this way with only one spin-orbit band parameter, there is as yet no experimental evidence in silicon or germanium to support a more complicated model.

Note added in proof. Recent optical measurements by Ghosh [Solid State Commun. **4**, 565 (1966)] and by Potter [Bull. Am. Phys. Soc. **12**, 320 (1967)] suggest that the spin-orbit splitting of the Γ_{15} conduction band is smaller than that for the $\Gamma_{25'}$ valence band. This would indicate that the next term in the Fourier expansion of $\mathcal{H}_{s\text{-}o}$ should be included.

At the Γ point, the $p_{3/2}$ levels are still fourfold degenerate. As we move away from the Γ point, as for example along the Λ or Δ axes, spin-orbit interaction lifts the degeneracy. In particular, at the L point, the two L_3 bands are each symmetrically split about their centers of gravity to a separation of approximately $\frac{2}{3}\Delta$. This separation between the components of the Λ_3 bands is approximately maintained for most of the distance along the Λ axes from L to Γ. Although the spin-orbit interaction lifts the degeneracy of the $p_{3/2}$ level along the Δ axis, the splitting in this case is very small, or approximately one order of magnitude smaller than the $p_{1/2}$-$p_{3/2}$ splitting at the Γ point. Nevertheless, this splitting is important in giving these levels nonzero slope at the X point. In fact, at X all the bands have X_5 symmetry. Spin-orbit interaction does not split the double degeneracy of the $E^{\pm}(X_5)$ levels. This degeneracy is required for the symmetry-type change $\Delta_6 \leftrightarrow \Delta_7$ in crossing the X point in the extended-zone scheme. Detailed results for these spin-orbit splittings throughout the Brillouin zone are given in Sec. III. The effect of spin-orbit interaction on the band curvatures or effective masses is also discussed there.

The treatment of the spin-orbit interaction given above is presented in the sense of a perturbation-theory expansion. Although this approach is probably the simplest to apply, it may not be appropriate if the spin-orbit interaction is sufficiently large so that perturbation theory is not rapidly convergent. If perturbation theory does not converge rapidly, then it may be necessary to construct a (16×16) effective-mass Hamiltonian $\mathcal{H}_T$ that includes the spin-orbit interaction from the beginning. In this case, the eight basis functions are

$$[s\uparrow, s\downarrow, p_{1/2}(\tfrac{1}{2}), p_{1/2}(-\tfrac{1}{2}), p_{3/2}(\tfrac{3}{2}), p_{3/2}(\tfrac{1}{2}), p_{3/2}(-\tfrac{1}{2}), p_{3/2}(-\tfrac{3}{2})],$$

and the Hamiltonian is written following Eq. (48) in terms of four (8×8) blocks $\mathcal{H}_T^{++}, \mathcal{H}_T^{+-}, \mathcal{H}_T^{-+}, \mathcal{H}_T^{--}$ as

$$\mathcal{H}_T(\mathbf{k}) = \begin{pmatrix} \mathcal{H}_T^{++}(\mathbf{k}) & \mathcal{H}_T^{+-}(\mathbf{k}) \\ \mathcal{H}_T^{-+}(\mathbf{k}) & \mathcal{H}_T^{--}(\mathbf{k}) \end{pmatrix}. \tag{52}$$

The symmetry types of the eigenvalues of $\mathcal{H}_T(\mathbf{k})$ are labeled by double-group representations of the cubic group,[45] rather than by the symmetry types given in Sec. IIA. Furthermore, a larger number of independent band parameters would be required for a Fourier expansion to second-neighbor interactions ($\alpha=2$). The reason more band parameters are required to describe $\mathcal{H}_T(\mathbf{k})$ when spin-orbit interaction is included *ab initio* is that the spin-orbit interaction couples different spin states. To say this another way, application of the inverse unitary transformation to $\tilde{\mathcal{H}}_0(\mathbf{k})$, $U^{+}\tilde{\mathcal{H}}_0(\mathbf{k})U$, results in a matrix which has only zero matrix elements connecting different spin states, as in Eq. (45). On the other hand, the matrix $U^{\dagger}\mathcal{H}_T(\mathbf{k})U$ will contain matrix elements connecting different spin states, and these matrix elements will involve band parameters different from the 13 parameters of Sec. IIA for $\alpha \leqslant 2$. Therefore, the perturbation-theory approach has the advantage of introducing fewer band parameters, but suffers from the disadvantage that the convergence of the perturbation theory is assumed. It has been found by direct calculation that for silicon and germanium, perturbation theory with one spin-orbit band parameter is sufficient. Perhaps for gray tin, where the spin-orbit interaction is larger, perturbation theory may not be sufficiently rapidly convergent, and the more general double-group approach would be necessary.

D. Dielectric Constant

Once the energy-band parameters which enter the effective-mass Hamiltonian are determined, explicit expressions for $E_n(\mathbf{k})$ are available. Since the band-parameter evaluation depends largely on the behavior of the energy bands in the vicinity of a few high-symmetry points, it is especially useful to apply these energy bands to study such phenomena as the frequency dependence of the dielectric constant which depends on the dispersion relations $E_n(\mathbf{k})$ throughout the entire Brillouin zone. The dielectric constant is sensitive to the band ordering, and therefore is useful in the identification of optical structure with a particular critical point.

The frequency-dependent dielectric constant is calculated in the effective-mass approximation using the expression of Ehrenreich and Cohen[51]:

$$\epsilon(\omega) = \epsilon_1 + i\epsilon_2 = 1 - m_0^{-1}\left(\frac{e}{\pi}\right)^2 \int d\mathbf{k} \sum_{n,n'} f_n(\mathbf{k}) f_{\mu n' n} \times (\omega - \omega_{nn'} + i/\tau_{nn'})^{-1}(\omega + \omega_{nn'} + i/\tau_{nn'})^{-1}, \tag{53}$$

in which $f_n(\mathbf{k})$ is the Fermi distribution function, and

$$f_{\mu n' n} = (2/\hbar m_0 \omega_{n' n})\,|\,p_{\mu n' n}\,|^2. \tag{54}$$

In this application of the dielectric-constant formula, the band indices n and n' are restricted to the eight bands which are explicitly treated by the Fourier-

[51] H. Ehrenreich and M. H. Cohen, Phys. Rev. **115**, 786 (1959).

expansion approach given in Sec. IIA. The energy difference between bands n and n' at an arbitrary point $\mathbf{k}$ is $\hbar\omega_{nn'}=E_n(\mathbf{k})-E_{n'}(\mathbf{k})$, and the energies $E_n(\mathbf{k})$ are found by solution of the eigenvalue problem of the Hamiltonian in Eq. (7). Since electronic transitions to other energy bands (e.g., d bands) are neglected in this calculation of the dielectric constant, quantitative agreement with experiment cannot be expected above photon energies at which such transitions become important, i.e., about 6 or 7 eV in germanium and $\sim$20 eV in silicon. In the spirit of the Fourier-expansion technique, only a limited number of bands are explicitly considered, and this group is chosen to include those bands which are most important within a few electron volts on either side of the Fermi level.

The $\mathbf{k}$ dependence of the momentum matrix element $p_{\mu n' n}$ in the μ direction between states n and n' is calculated through use of the effective-mass approximation by taking appropriate derivatives with respect to $\mathbf{k}$ of the effective-mass Hamiltonian according to Eqs. (44a) and (44b). In this way, both diagonal and off-diagonal matrix elements are calculated, and it is found that the magnitude of these matrix elements is strongly $\mathbf{k}$ dependent.

In the actual calculation, the relaxation time $\tau_{nn'}$ was assumed to be independent of the band indices n and n', and to be independent of the photon energy $\hbar\omega$. This is a great oversimplification, since the relaxation time must vary from band to band as well as from point to point in the Brillouin zone. Furthermore, the greater availability of final states with increasing photon energy is expected to result in a decrease in $\tau_{nn'}$ with increasing photon energy. Furthermore, $\tau_{nn'}$ would not be expected to be a smooth function of photon energy because of sudden onsets of interband relaxation processes with increasing $\hbar\omega$. The actual value taken for $\tau_{nn'}$ is characteristic of a general point in the Brillouin zone, and is therefore smaller than the values characteristic of critical points, where certain relaxation processes are forbidden. As long as $\omega\tau_{nn'}\gg 1$, the magnitude of $\tau_{nn'}$ has no important effect on ϵ_2, except in the immediate vicinity of optical structure. However, $\tau_{nn'}$ has a greater effect on ϵ_1, particularly in the neighborhood of the optical structure. In fact, the observed maximum in ϵ_1 can be used in the actual selection of $\tau_{nn'}$ for the calculation. With this selection, the frequency dependence of ϵ_2 is only a function of the band parameters, and no normalization adjustments need be introduced.

The actual $\mathbf{k}$ integration in Eq. (53) was carried out using a Monte Carlo procedure[10] to select $\mathbf{k}$ points. Since the calculation is limited to the interband contribution to the dielectric constant, it is adequate to take the Fermi function $f_n(\mathbf{k})=0$ or 1, respectively, for unoccupied or occupied bands, thereby neglecting intrinsic excitation or doping effects in semiconductors. To simplify the actual calculation, the effects of spin-orbit interaction are neglected. Explicit results for the frequency dependence of the real and imaginary parts of the dielectric constant in silicon and germanium are presented in Sec. III. It is found that the calculated curves provide a surprisingly good representation of the experimental data, for Fourier-expanded energy bands which do not contain terms beyond next-nearest-neighbor interactions, i.e., $\alpha\leq 2$.

III. BAND-PARAMETER DETERMINATION IN SILICON AND GERMANIUM

The energy bands of the diamond lattice are the eigenvalues of the effective-mass Hamiltonian presented in Sec. II. These energy bands are completely determined over the entire Brillouin zone, once the pertinent band parameters or Fourier coefficients have been evaluated. The number of these band parameters depends upon the number of terms which are retained in the Fourier expansion. If the integer α denotes the αth nearest-neighbor interaction, then there are two independent band parameters for $\alpha=0$, four for $\alpha=1$, seven for $\alpha=2$, and seven for $\alpha=3$. In the case of silicon and germanium, there are more than enough experiments to determine all the Fourier coefficients for $\alpha\leqslant 2$, but not quite enough to evaluate all of the coefficients for $\alpha=3$. It is found that by including only those 13 coefficients for which $\alpha\leqslant 2$, a very good representation of the energy bands is obtained, consistent with most of the experimental results to within their reported errors. The band-parameter determination described here is thus an attempt to obtain the optimum representation of the energy bands without introducing any terms for $\alpha\geqslant 3$. Nevertheless, these 13 constants are overdetermined by the presently available experimental data, and it is found that terms in $\alpha=3$ are ultimately needed to trim up these energy bands to yield quantitative agreement with certain experiments. Such an extension of the present analysis is not difficult and is developed in Appendix A. However, no explicit evaluation of the band parameters for $\alpha\geqslant 3$ is given in the present work.

In carrying out this band-parameter determination, more emphasis has been placed upon the frequency dependence of the complex dielectric constant than upon some of the less well-identified optical transitions. It is found that in silicon and germanium, the dielectric constant is more sensitive to the energy bands over a large volume of the Brillouin zone than it is to the bands in the vicinity of just a few critical points. Since it is desirable to determine the frequency dependence of the dielectric constant, it is fortunate that the Fourier-expansion technique permits an accurate and rapid calculation of this quantity.

In the case of silicon and germanium, the effect of spin-orbit interaction can be adequately handled by the perturbation theory approach given in Sec. IIC and, therefore, only one additional band parameter need be

TABLE VI. Dependence of physical quantities on band parameters.

	$\gamma_{0,1}$	$\gamma_{0,2}$	$\gamma_{1,1}$	$\gamma_{1,2}$	$\gamma_{1,3}$	$\gamma_{1,4}$	$\gamma_{2,1}$	$\gamma_{2,2}$	$\gamma_{2,3}$	$\gamma_{2,4}$	$\gamma_{2,5}$	$\gamma_{2,6}$	$\gamma_{2,7}$
$E(\Gamma_1)$	1												
$E(\Gamma_{2'})$	1		−8										
$E(\Gamma_{15})$		1											
$E(\Gamma_{25'})$		1		−8									
$E^+(X_4)-E^-(X_4)$					8								
$E(L_3)-E(L_{3'})$				4	4								
$Q(\Gamma_{25'})$				1	−1			−4	2		1		
$E^+(X_4)+E^-(X_4)$		2		−8				−16			−8		
$E^+(X_1)+E^-(X_1)$	1	1	−4	−4			−8	−8			8		
$E(L_3)+E(L_{3'})$		2		−8				−12	4				
$E^+(L_1)+E^-(L_1)$	1	1	−6	−2	−4		−6	−6	−4				
$E^+(L_{2'})+E^-(L_{2'})$	1	1	−2	−6	4		−6	−6	−4				
$E''(\Gamma_{2'})+2L(\Gamma_{25'})$			1	1			−4	−4			4		
$E''(\Gamma_{2'})$	√	√	√	√		√	√			√			
$L(\Gamma_{25'})$	√	√	√	√		√		√		√	√		
$M(\Gamma_{25'})$				√	√			√		√			
$E(X_1)$	√	√	√	√		√	√	√			√		
$E_l'(X_1),E_l''(X_1)$	√	√	√	√		√	√	√		√	√		
$E(L_1),E(L_{2'})$	√	√	√	√	√	√	√	√	√			√	
$E_l''(L_1)$	√	√	√	√	√	√	√	√	√	√		√	
$E_t''(\Delta_1),E_t''(L_1)$	√	√	√	√	√	√	√	√	√	√	√	√	√

introduced. This parameter is determined directly and independently of the other band parameters. In germanium, the optical doublet structure identified with the transition $E(\Gamma_{25'})\rightarrow E(\Gamma_{2'})$ yields the spin-orbit band parameter directly.[52–54] An accurate value for this parameter in silicon has been obtained from analysis of the impurity level spectra of acceptors.[55]

If the Fourier series is terminated with terms involving next-nearest-neighbor interactions, 13 band parameters need to be determined. One parameter is immediately evaluated by fixing the zero of energy at the top of the valence band $E(\Gamma_{25'})$, thereby yielding the relation $\gamma_{0,2}=8\gamma_{1,2}$. It is, therefore, necessary to select 12 pieces of experimental information, such that these data yield a system of 12 independent equations in the 12 unknowns. The selection of independent experiments can be accomplished by use of Table VI, which summarizes the band-parameter dependence of several energy bands and their derivatives at various high-symmetry points and axes in the Brillouin zone. In the upper half of this table, explicit values for the coefficients are given for those physical quantities which have a linear dependence on only a few band parameters. On the other hand, those physical quantities that have a more complicated dependence on the band parameters $\gamma_{i,j}$ are listed in the lower half of the table. In this part of the table a band-parameter dependence is indicated by a check. Derivatives of the energy bands are denoted by primes and are taken in the longitudinal (l) and transverse (t) directions with respect to the Δ and Λ axes.

Fortunately, a vast quantity of experimental information is available for both silicon and germanium, so that it is easy to find 12 independent experiments. The selection of a particular experiment is guided not only by the accuracy of the measurement, but also by the number and type of the dependent band parameters. For example, the optical structure identified with the $E(L_{3'})\rightarrow E(L_3)$ transition is a particularly convenient experiment to use, since it depends only upon 2 band parameters $\gamma_{1,2}$ and $\gamma_{1,3}$; on the other hand, the measurement of the transverse cyclotron mass at the L point in germanium is more difficult to apply, since it depends on all 12 band parameters. As the availability and precision of experimental information increases, a better selection of experiments can be made. Not only can the band parameters for $\alpha\leqslant 2$ be determined more precisely, but a more accurate representation of the energy bands can be achieved through the determination of higher-Fourier coefficients, such as the band parameters for $\alpha=3$.

It should be emphasized that there is an element of subjectivity involved in the choice of the 12 experiments which are to be used in the band-parameter determination. These constants are overdetermined by the available experimental data, and no set of band parameters exactly satisfies all the experimental information to within the quoted errors. In this particular determination the frequency dependence of the complex dielectric constant has been emphasized. If on the other hand, photoemission results had received more atten-

[52] M. V. Hobden, J. Phys. Chem. Solids **23**, 821 (1962).
[53] B. O. Seraphin and R. B. Hess, Phys. Rev. Letters **14**, 138 (1965).
[54] S. H. Groves, C. R. Pidgeon, and J. Feinleib, Phys. Rev. Letters **17**, 643 (1966).
[55] S. Zwerdling, K. J. Button, B. Lax, and L. M. Roth, Phys. Rev. Letters **4**, 173 (1960).

tion than the dielectric constant, a slightly different set of band parameters would have been obtained. Since a particular band-parameter determination can be carried out in less than 1 min on a high-speed digital computer, it is possible to vary the set of independent experiments. It is also easy to examine various band orderings suggested by optical experiments and to investigate the internal consistency of a particular set of experimental data.

The present band-parameter determination for silicon and germanium is based on eight similar measurements and four dissimilar though somewhat related measurements. The experiments common to both materials include soft x-ray-emission studies to yield $\gamma_{0,1}$, critical-point identification of optical transitions between $E(\Gamma_{25'})\rightarrow E(\Gamma_{2'})$, the $E(L_{3'})\rightarrow E(L_3)$, and the $E(L_{3'})\rightarrow E(L_1)$, as well as cyclotron-resonance measurements of the three effective-mass quantities L, M, and N of the degenerate-valence band $E(\Gamma_{25'})$. The separation $E^+(X_1)-E^-(X_4)$ was adjusted to yield agreement between the calculated and observed energy for the maximum in ϵ_2. In the case of silicon, the remaining four experiments involve the lowest-conduction band $E(\Delta_1)$. The energy $E(\Delta_1)$ is determined from optically induced transitions across the indirect gap $E(\Gamma_{25'})\rightarrow E(\Delta_1)$.[56] The location of the energy minimum along the Δ_1 axis is found by analysis of the spacial variation of the electron wave functions about donor-impurity states.[57] The band curvatures about the energy extremum, both along the Δ_1 axis and perpendicular to it, are determined from the longitudinal and transverse cyclotron effective masses obtained from cyclotron-resonance measurements on electrons.[14,15] In the case of germanium, use is made of the longitudinal and transverse cyclotron masses of the lowest conduction band at the L point,[14,15] the spherically symmetric effective mass at $E(\Gamma_{2'})$[54,58] and the energy at the conduction-band minimum $E(L_1)$.[59]

In both materials, the parameter $\gamma_{0,1}$, which defines the position of the valence s band at $\mathbf{k}=0$, is determined from soft x-ray-emission studies,[21,22] which provide a measurement of various bandwidths and are particularly valuable for the investigation of valence bands far from the Fermi level. It is found that this energy band does not interact strongly with any of the other bands, so that the band structure as a whole is quite insensitive to a sizeable (e.g., 20% variation of this parameter). Valence bandwidths of 16.7 eV and 7.0 eV have been reported for silicon and for germanium, respectively.[21,22] In Fig. 2, it is seen that the valence s band is a relatively flat band and shows only a small amount of $\mathbf{k}$ dependence.

The parameter $\gamma_{1,1}$ depends upon the separation of the s bands at the Γ point, and is determined by identification of optical structure with an interband transition $E(\Gamma_{25'})\rightarrow E(\Gamma_{2'})$. Because of the spin-orbit splitting of the valence band $E(\Gamma_{25'})$, this transition is expected to be a doublet with an energy separation of Δ. In the case of germanium, this doublet structure is so well resolved that this transition can be unambigously identified. The structure is observable in both optical absorption[52] and electroreflectance measurements,[53,54] yielding a room temperature separation of 0.803 ± 0.003 eV[52–54] from the conduction s bands to the $p_{3/2}$ valence level and of 1.09 ± 0.01 eV[52–54] to the $p_{1/2}$ valence level at the Γ point. Therefore, in germanium, the spin-orbit parameter is found to be $\Delta=0.29\pm0.01$ eV, and since the $E(\Gamma_{25'})$ level is at the center of gravity of the $p_{3/2}$ and $p_{1/2}$ valence levels, we have $E(\Gamma_{2'})-E(\Gamma_{25'})=0.900\pm0.006$ eV.

On the other hand, the spin-orbit splitting in silicon is much smaller, so that the identification of a doublet structure with the $E(\Gamma_{25'})\rightarrow E(\Gamma_{2'})$ transition is somewhat ambiguous. For this reason, the dependence of the dielectric constant on the separation $E(\Gamma_{2'})-E(\Gamma_{25'})$ was used to help with the identification of this transition. Characteristic features in both the real and imaginary parts of the dielectric constant for silicon are sensitive to the separation $E(\Gamma_{2'})-E(\Gamma_{25'})$. The energy dependence of the real part ϵ_1, shown in Fig. 3(a), exhibits a broad shoulder between 3.5 and 3.8 eV, while the imaginary part ϵ_2, shown in Fig. 3(b), has a fairly sharp minimum near 3.65 eV.[18] By placing $E(\Gamma_{2'})-E(\Gamma_{25'})=3.75\pm0.20$ eV, these features in the calculated curves for ϵ_1 and ϵ_2 could be obtained at the appropriate energies. Relatively weak optical structure has been observed at 3.7 eV[60] and, in addition, a small peak in the photoemission yield has been reported at this photon energy.[19] Various identifications for these structures have been given in the literature.[4,6] Since there are probably several critical points in the joint density of states at about this energy, the identification of this structure with $E(\Gamma_{2'})-E(\Gamma_{25'})$ cannot be made unambigously.

The determination of the spin-orbit band parameter in silicon is not made from analysis of any doublet structure connected with the transition $E(\Gamma_{25'})\rightarrow E(\Gamma_{2'})$. On the other hand, a precise value of $\Delta=0.0441\pm0.0004$ eV has been deduced from analysis of the infrared spectrum of electronic transitions from the valence bands to acceptor impurity levels.[55]

With the identification of the $E(\Gamma_{25'})\rightarrow E(\Gamma_{2'})$ transition, and the zero of energy taken at the $E(\Gamma_{25'})$ level, the value of $\gamma_{1,1}$ is simply given by Eq. (16) as

$$\gamma_{1,1}=-\tfrac{1}{8}[E(\Gamma_{2'})-\gamma_{0,1}]. \tag{55}$$

[56] G. G. Macfarlane, T. P. McLean, J. E. Quarrington, and V. Roberts, Phys. Rev. **111**, 1245 (1958).
[57] G. Feher, Phys. Rev. **114**, 1219 (1959) and J. Phys. Chem. Solids **8**, 486 (1959).
[58] B. Lax and S. Zwerdling, *Progress in Semiconductors* (John Wiley & Sons, Inc., New York, 1960), Vol. 5, p. 221.
[59] W. E. Engeler, M. Garfinkel, and J. J. Tiemann, Phys. Rev. Letters **16**, 239 (1966).
[60] J. Tauc and A. Abraham, J. Phys. Chem. Solids **20**, 190 (1961).

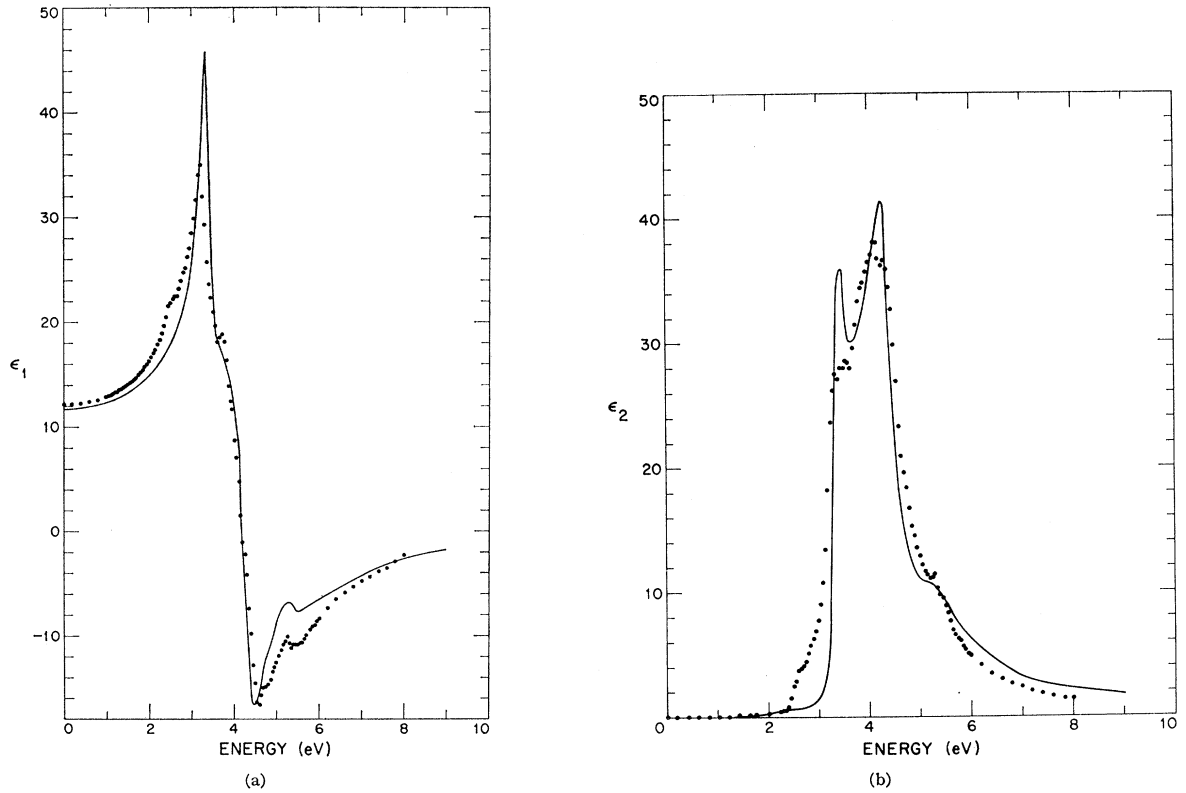

FIG. 3. Frequency dependence of the real (ϵ_1) and imaginary (ϵ_2) parts of the dielectric constant for silicon. The solid curves represent the experimental determination by Philipp and Ehrenreich, (see Ref. 18) while the dots are calculated by a Monte Carlo procedure using 10 000 points and $\tau=2\times10^{-14}$ sec.

There are two other band parameters, $\gamma_{1,2}$ and $\gamma_{1,3}$ which can be readily evaluated. If a characteristic optical structure can be identified with the interband transition $E(\Gamma_{25'})\rightarrow E(\Gamma_{15})$, then using Eq. (16), $\gamma_{1,2}$ is simply related to this energy separation, according to the relation $\gamma_{1,2}=\frac{1}{8}[E(\Gamma_{15})-E(\Gamma_{25'})]$. The characteristic optical structure expected for this transition is a triplet, with each of the two extreme components separated by about the spin-orbit parameter Δ from the central component. When the present energy-band determination was undertaken, it was felt that the $E(\Gamma_{25'})\rightarrow E(\Gamma_{15})$ transition was not sufficiently well-identified to be used for experimental data in the band-parameter evaluation. However, as a result of the dielectric-constant calculation, it was found that certain features in the dielectric constant are closely associated with this transition. The sharp rise in ϵ_2 for silicon near 3.1 eV,[18] is sensitive to the separation of $E(\Gamma_{15})-E(\Gamma_{25'})$. In the present calculation for silicon, this separation is determined from other experiments, and unless Fourier coefficients for $\alpha=3$ are introduced, the separation $E(\Gamma_{15})-E(\Gamma_{25'})$ cannot easily be made greater than 2.6 eV. By increasing the $E(\Gamma_{15})-E(\Gamma_{25'})$ separation by about 10–20% through use of higher-Fourier coefficients, an improvement in the leading edge would be achieved. Furthermore, the $E^{+}(\Lambda_1)-E^{-}(\Lambda_3)$ separation in ϵ_2 would then become more closely constant at about 3.2 eV from Γ to L, and an increase would result in the intensity of the calculated peak at 3.5 eV.

In the case of germanium, the separation $E(\Gamma_{15})-E(\Gamma_{25'})$ is closely correlated with the structure in ϵ_1 and with the onset of a rise in ϵ_2 observed in the vicinity of 3.0 eV.[18] Optical structure has been observed in this energy range in the reflectance,[18] the piezoreflectance[2] and the electroreflectance,[53] and has been identified with the $E(\Gamma_{25'})\rightarrow E(\Gamma_{15})$ transition.[6] In fact, the electroreflectance data of Seraphin and Hess[53] show a triplet structure with each component separated by approximately Δ, the appropriate separation at the Γ point. In the present treatment, this separation has not been used explicitly in the band-parameter determination; but instead, this quantity has been evaluated from $\gamma_{1,2}$, which in turn (as explained below) has been determined from the energy bands at the L point and from the effective-mass parameters associated with the degenerate valence band $E(\Gamma_{25'})$. With these identifications of $E(\Gamma_{15})-E(\Gamma_{25'})$, approximately the same separation is found for both silicon and germanium.

In the case of both silicon and germanium, various authors[4,6,10–12] have identified certain optical structures with the $E(L_{3'})\rightarrow E(L_3)$ transition, and this energy separation conveniently depends upon only two band

parameters. From Eq. (33), it follows that

$$E(L_3)-E(L_{3'})=4(\gamma_{1,2}+\gamma_{1,3}). \quad (56)$$

The characteristic optical structure associated with this transition is a triplet, with each component separated by $\sim\frac{2}{3}\Delta$, where Δ is the spin-orbit splitting at the Γ point. No such triplet structure has yet been resolved within the linewidth, and, therefore, the identification of the structure at 5.4 ± 0.1 eV in silicon[18,3,61] and at 5.5 ± 0.1 eV in germanium[18,62] is ambiguous. Using the band-parameter-determination procedure described here, it is found that the qualitative characteristics of the energy bands throughout the Brillouin zone and the associated dielectric constant are not significantly affected by a ±0.4 eV variation of the energy difference $E(L_3)-E(L_{3'})$.

Equation (56) provides one relation involving the band parameters $\gamma_{1,2}$ and $\gamma_{1,3}$. A second equation in these two unknowns is obtained using Eqs. (17), (33), (41), and (42), and can be written as

$$M-\tfrac{1}{4}E^-(X_4)=M+Q-E(L_{3'})=-\tfrac{1}{2}\gamma_{1,2}+\gamma_{1,3}-\frac{(\gamma_{1,3})^2}{2\gamma_{1,2}}, \quad (57)$$

in which the quantities M and Q are appropriate to the valence band $E(\Gamma_{25'})$. Thus, simultaneous solution of Eqs. (56) and (57) yields $\gamma_{1,2}$ and $\gamma_{1,3}$. The restriction $\gamma_{1,3}>0$ of Eq. (26) results in only one physically acceptable solution. The values for M and Q are obtained from analysis of cyclotron-resonance experiments on the holes associated with the $E(\Gamma_{25'})$ valence band. The values are $M=-1.56\pm0.18$ eV and $Q=-0.63\pm0.58$ eV for silicon[14–16,63] and $M=-2.21\pm0.18$ eV and $Q=-0.07\pm0.84$ eV for germanium.[14,15,17,63] Since the value of Q is not well established experimentally, the energy $E^-(X_4)$ is used to determine $\gamma_{1,2}$ and $\gamma_{1,3}$, while Q is evaluated according to the relation $Q=E(L_{3'})-\frac{1}{4}E^-(X_4)$. The energy $E^-(X_4)$ is obtained from determination of the energy separation $E^+(X_1)-E^-(X_4)$ and of the energy $E^+(X_1)$. For silicon, the lowest conduction band is in the vicinity of the X point, so that $E^+(X_1)$ is obtained from well-established measurements of the indirect band gap $E(\Delta_1{}^{\min})$, of the location of the conduction-band minima at $\Delta_1{}^{\min}$, and of the longitudinal electron cyclotron mass $m_l{}^*/m_0$ at $\Delta_1{}^{\min}$. Assuming parabolic bands in the neighborhood of $\Delta_1{}^{\min}$, $E^+(X_1)$ is related to the energy at the band extremum by

$$E^+(X_1)=E^+(\Delta_1{}^{\min})+\frac{\hbar^2\pi^2(1-\delta_1)^2}{2m_l{}^*a^2}, \quad (58)$$

where $E^+(\Delta_1{}^{\min})-E(\Gamma_{25'})=1.156$ eV at 4.2°K and 1.114 eV at 291°K.[56] The conduction-band minima are located at $ka=\pi\delta_1$, where $\delta_1=0.85\pm0.03$,[57] and the longitudinal electron cyclotron mass is $m_l{}^*/m_0=0.97\pm0.02$ at $\Delta_1{}^{\min}$.[14,15] The distance a for silicon is 2.71 Å. Once the energy $E^+(X_1)$ is determined, the energy $E^-(X_4)$ follows from a knowledge of the separation of $E^+(X_1)-E^-(X_4)$. Since the X point is generally not a critical point in the joint density of states, it is not possible to make an unambiguous identification of optical structure with the $E^-(X_4)\rightarrow E^+(X_1)$ transition. However, because of the flatness of the energy bands in the vicinity of the X point, various critical points exist in this region of the Brillouin zone. These flat bands contribute strongly to the dielectric constant and are responsible for the large maximum in ϵ_2 in the neighborhood of 4.2 eV. The value for the separation $E^+(X_1)-E^-(X_4)$ has been adjusted to obtain a fit for the energy of the 4.2-eV peak of the frequency-dependent dielectric constant.[18] Although $E^+(X_1)-E^-(X_4)$ was taken at 3.75 eV for silicon, a variation of ±0.2 eV could be made in this quantity without seriously affecting the dielectric constant. The energy $\frac{1}{4}E^-(X_4)$ was taken as -0.63 ± 0.07 eV. However, since the coefficient in front of $E^-(X_4)$ in Eq. (57) is $\frac{1}{4}$, and $|M|\gg|\frac{1}{4}E^-(X_4)|$, the uncertainty in $E^-(X_4)$ has less effect upon the determination of $\gamma_{1,2}$ and $\gamma_{1,3}$ than does the uncertainty in M.

The level $E^+(X_1)$ has not been directly studied in germanium. Studies of the reflectivity from germanium-silicon alloys[60,64] have been interpreted to yield only a small variation in the energies of $E^+(X_1)$ and $E^-(X_4)$ in going from pure silicon to pure germanium. To allow for experimental uncertainties and errors in identification of interband transitions, a wide variation was made of the experimental data pertinent to Eqs. (56) and (57), and only small variations in $\gamma_{1,2}$ and $\gamma_{1,3}$ resulted.

One useful application of the Fourier-expansion description of the energy bands in a solid is exemplified in the relation $Q=E(L_{3'})-\frac{1}{4}E^-(X_4)$ given by Eq. (57). Here, an energy-band curvature at the Γ point is related to the energy which that band attains at distant points L and X in the Brillouin zone. By including only terms up to $\alpha\leqslant2$ in the Fourier expansion, these band parameters are overdetermined, and quantities such as $Q(\Gamma_{25'})$ and the separation $E(\Gamma_{15})-E(\Gamma_{25'})$, discussed previously, cannot be adjusted freely, i.e., independently of each other.

For both silicon and germanium, experimental data is available which determine the energy $E(L_{3'})$ and $Q(\Gamma_{25'})$ is thereby evaluated. By studying both the spectral distribution of the quantum yield and the kinetic-energy distribution of the emitted electrons on photoemission from silicon,[19] it has been possible to estimate both the initial and final states associated with the 5.4 eV interband transition. Since this transition has

[61] A. K. Ghosh, Phys. Letters **23**, 36 (1966).
[62] A. K. Ghosh, Solid State Commun. **4**, 565 (1966).
[63] J. J. Stickler, H. J. Zeiger, and G. S. Heller, Phys. Rev. **127**, 1077 (1962).
[64] J. Tauc, in *Proceedings of the International Conference on the Physics of Semiconductors, Exeter* (The Institute of Physics and The Physical Society, London, 1962), p. 333.

been identified as an $E(L_{3'}) \rightarrow E(L_3)$ transition,[4,6,10–12] the photo-emission results have been interpreted to yield $E(L_{3'}) = -1.5 \pm 0.2$ eV and $E(L_3) = 3.8 \pm 0.2$ eV.[19] With these data, the valence-band effective-mass parameter Q for silicon is estimated to be $Q(\Gamma_{25'}) = -0.85 \pm 0.25$ eV.

In the case of germanium, the position of the $E(L_{3'})$ level is even more firmly established. By measurements such as the piezotransmission,[59] an accurate room-temperature value for $E(L_1) = 0.6643 \pm 0.0005$ eV is obtained. The $E(L_1)$ level is a nondegenerate level, and, therefore, is essentially unaffected by the spin-orbit interaction. The $E(L_{3'})$ level is then determined by identification of the characteristic doublet optical structure at 2.11 ± 0.01 eV and 2.33 ± 0.01 eV with the $E(L_{3'}) \rightarrow E(L_1)$ transition.[2,18,53,62,65] Since the separation of this doublet is 0.22 ± 0.02 eV, which is approximately $\frac{2}{3}\Delta$ for germanium, this splitting is attributed to spin-orbit interaction. From these results it follows that the center of gravity for the $E(L_{3'})$ levels is at -1.56 ± 0.02 eV. These arguments yield an estimate for $Q(\Gamma_{25'}) = -0.80 \pm 0.20$ eV in germanium.

Whereas the parameters $\gamma_{0,1}$, $\gamma_{1,1}$, $\gamma_{0,2}$, $\gamma_{1,2}$, and $\gamma_{1,3}$ can be evaluated quite simply from experimental data, the remaining parameters are evaluated by solving equations of higher order. Since the available experimental information differs somewhat in silicon and germanium, different procedures were used in the band-parameter determination for the remaining constants.

For silicon, the four variables $\gamma_{1,4}$, $\gamma_{2,4}$, $\gamma_{2,1}$, and $\gamma_{2,25} = (\gamma_{2,2} - \gamma_{2,5})$ are evaluated from solution of four coupled equations involving the energy and location of the conduction-band minimum $E(\Delta_1^{\min})$, the longitudinal cyclotron effective mass at $\Delta_1^{\min}$ and the effective-mass quantity $L(\Gamma_{25'})$ of the valence band. The details involved in the solution of these coupled equations is given in Appendix B. Values for $\gamma_{2,2}$ and $\gamma_{2,5}$ are then found directly by the simultaneous solution of the equation $\gamma_{2,25} = \gamma_{2,2} - \gamma_{2,5}$ with the equation for the effective-mass quantity $M(\Gamma_{25'})$ given by Eq. (41). After these band parameters have been evaluated, the parameter $\gamma_{2,3}$ is simply determined from the effective-mass parameter $Q(\Gamma_{25'})$ by use of Eq. (42). Since Q is not well determined experimentally, it is most conveniently evaluated by the first relation in Eq. (57), as discussed above.

The parameter $\gamma_{2,6}$ is determined by the energy of the $E^+(L_1)$ conduction band. Since this energy is not measured directly, it is found from the energy separation $E^+(L_1) - E(L_{3'})$ and from the energy of the $E(L_{3'})$ level. The sharp edge in the imaginary part of the dielectric constant ϵ_2 at 3.2 eV,[18] shown in Fig. 3(b), is closely correlated with the $E(L_{3'}) \rightarrow E^+(L_1)$ transition and places the energy separation $E^+(L_1) - E(L_{3'})$ at 3.2 ± 0.1 eV. Since the energy $E(L_{3'}) = 1.5 \pm 0.2$ eV is known from photoemission studies,[19] $E^+(L_1)$ is readily evaluated. From Eqs. (31) and (32) it is seen that the $E^+(L_1)$ and $E^+(L_{2'})$ levels depend only upon the parameters $\gamma_{2,6}$ and other quantities that have already been evaluated. Solution of Eq. (31) for $\gamma_{2,6}$ is thus accomplished with the restriction that the resulting $E^+(L_1)$ level lie lower than the $E^+(L_{2'})$ level. With this identification, it is found that as we move away from the L point, the energy-band separation of about 3.2 eV is maintained over a relatively large volume of the Brillouin zone about the Λ axis. This flatness of the $E^+(L_1)$ band is responsible for the large contribution to ϵ_2 from this region of the Brillouin zone. However, it is found that this contribution to the ϵ_2 edge is not sufficiently large, so that some intensity must come from elsewhere. For example, by increasing the $E(\Gamma_{15}) - E(\Gamma_{25'})$ separation, an improvement can be obtained both in the shape of the leading edge and in the height of the 3.5-eV peak in ϵ_2. It should be emphasized that contributions are made to this 3.5-eV peak from other points in the Brillouin zone, such as along the Δ axis.

The remaining parameter $\gamma_{2,7}$ is evaluated by fitting the curvature of the lowest conduction band about the energy minimum to the observed transverse cyclotron effective-mass $m_t^*/m_0 = 0.19 \pm 0.01$.[14,15] Since the related energy band curvature depends in a complicated way upon all the band parameters, a simple numerical fitting procedure was found to be most convenient. Since few of the experimentally observed quantities depend upon the value of this parameter, the characteristic features of the energy bands are relatively insensitive to $\gamma_{2,7}$.

To summarize these results, the values obtained for the band parameters in silicon are listed in Table VII. In this table, the six band parameters corresponding to zeroth and nearest-neighbor interactions are more accurately determined than are the seven parameters for next-nearest-neighbor interactions. These seven parameters, for which $\alpha = 2$, are relatively small and have a correspondingly smaller effect on the energy bands. In this table, the band parameters are listed in units of both Ry and eV. The values in the rydberg

TABLE VII. Band parameters for Si and Ge.

Parameter	Si		Ge	
	Ry	eV	Ry	eV
$\gamma_{0,1}$	−1.2300	−16.73	−0.5300	−7.21
$\gamma_{0,2}$	0.1787	2.43	0.2089	2.84
$\gamma_{1,1}$	−0.1881	− 2.56	−0.0745	−1.01
$\gamma_{1,2}$	0.0223	0.30	0.0261	0.35
$\gamma_{1,3}$	0.0752	1.02	0.0751	1.02
$\gamma_{1,4}$	−0.0977	− 1.33	−0.0728	−0.99
$\gamma_{2,1}$	0.0555	0.75	0.0312	0.42
$\gamma_{2,2}$	0.0042	0.06	0.0064	0.09
$\gamma_{2,3}$	0.0137	0.19	0.0162	0.22
$\gamma_{2,4}$	0.0103	0.14	0.0286	0.39
$\gamma_{2,5}$	−0.0147	− 0.20	−0.0128	−0.17
$\gamma_{2,6}$	−0.0359	− 0.49	−0.0179	−0.24
$\gamma_{2,7}$	−0.0232	− 0.32	−0.0304	−0.41
Δ	0.0032	0.044	0.0213	0.290

[65] K. L. Shaklee, F. H. Pollak, and M. Cardona, Phys. Rev. Letters **15**, 883 (1965).

units are quoted to one more place than in the eV units, not because there is any significance in this last figure, but rather because this number of figures was used in the computation.

The actual errors associated with the band parameters of Table VII are rather difficult to determine. If, for example, one of the experiments used in the band-parameter determination were to be carried out to greater accuracy, then not only one, but several (or maybe all) of the band parameters would be affected, the percentage change in the second-neighbor terms being greater than in the corresponding nearest-neighbor Fourier coefficient. Furthermore, the extension of the Fourier expansion to include third-neighbor interactions would also modify the Fourier coefficients in this table, the largest changes again occurring for the second-neighbor terms. No particular physical importance is attached to the value of any of these band parameters, but rather to the positions and curvatures of the energy bands.

In Table VIII, certain band curvatures and effective masses are listed and the corresponding experimental values are included if they have been measured. Results are given for all bands at the Γ, L, and X points, and for the nondegenerate $E^+(\Delta_1)$ at the conduction-band minimum; these results include the effect of spin-orbit interaction. The band curvatures for the degenerate valence and conduction bands at Γ are tabulated in the notation conventionally used in the literature,[14]

$$E^{\pm}(\mathbf{k})=E(0)+\frac{\hbar^2}{2m_0}\times\{Ak^2\pm[B^2k^4+C^2(k_x^2k_y^2+k_y^2k_z^2+k_x^2k_z^2)]^{1/2}\}, \quad (59)$$

whereby

$$A=\tfrac{1}{3}(L'+2M'),\quad B=\tfrac{1}{3}(L'-M'),\quad C=[\tfrac{1}{3}\{(N')^2-(L'-M')^2\}]^{1/2}, \quad (60)$$

and the L', M', and N' are related to the L, M, N, and Q used in this paper in Eqs. (36) and (42). The constants A, B, and C for the Γ point listed in Table VIII are determined by application of Eq. (59) which gives $E(\mathbf{k})$ including the effect of spin-orbit interaction. If, on the other hand, these constants has been determined from Eq. (60), and then from Eqs. (40)–(42) using the band parameters of Table VII, slightly different values would result, since these formulas do not explicitly include the effect of spin-orbit interaction.[66]

At the L point, the band degeneracies are lifted by the spin-orbit interaction, so that the band curvatures can be described by simple longitudinal and transverse effective masses. However, the curvatures at the X point cannot be described by simple effective masses.

[66] G. F. Dresselhaus, Ph.D. thesis, University of California, 1955 (unpublished).

When spin-orbit interaction is included, all the energy bands approach X with nonzero slope and are doubly degenerate just at the X point, where they are described by X_5 symmetry. The X point is, therefore, generally not a critical point in the joint density of states and is not a particularly interesting point in the Brillouin zone. Nevertheless, there has been much discussion and confusion about this matter in the literature and, therefore, $\mathbf{k}\cdot\mathbf{p}$ expansions for the energy bands about X are included in this paper. The $\mathbf{k}\cdot\mathbf{p}$ expansion is of the form

$$E^{\pm}(\mathbf{k})=E(X_5)\pm E'(X_5)(ak_x-\pi)+\frac{\hbar^2}{2a^2m_l^*}(ak_x-\pi)^2+\frac{\hbar^2}{2m_0}\times\{\mathfrak{A}(k_y^2+k_z^2)\pm[\mathfrak{B}^2(k_y^2+k_z^2)^2+\mathfrak{C}^2k_y^2k_z^2]^{1/2}\}. \quad (61)$$

At the X points, the band curvatures and slope depend on five quantities for which values are given in Table VIII. For the two X_4 levels, which without spin-orbit interaction have zero slope at X, the slope parameters $E'(X_5)$ are very small compared with the values obtained for the X_1 levels, which have nonzero slopes even without spin-orbit interaction.

Since many of the entries in Table VIII have not yet been experimentally determined, this table could be useful in planning certain optical and magneto-optical experiments. Band curvatures are generally more sensitive to higher-Fourier coefficients than are the energy levels. Therefore, neglect of Fourier-expansion coefficients for $\alpha\geqslant 3$ could result in significant errors in the calculated effective-mass parameters. The experimental data for silicon overdetermines the band parameters for $\alpha\leqslant 2$, and it is not possible to simultaneously satisfy all of the experimental data. Since the truncated Fourier series provides a better representation for the energy bands than for their curvatures, the quoted experimental errors for the energy levels were adhered to more closely than the corresponding errors for the effective-mass parameters in carrying out the band-parameter determination.

The energy bands along about 10 high-symmetry directions in the Brillouin zone were studied in detail and the results for a few of the more important axes in silicon are shown in Fig. 2. These bands are generally in qualitative agreement with the energy bands calculated by other techniques,[6,12] though quantitative differences occur. It is of interest to observe that the separations $E^+(\Delta_1)-E^-(\Delta_3)$ and $E^+(\Delta_1)-E^-(\Delta_5)$ are approximately constant over much of the Λ and Δ axes, respectively. The presence of nearly parallel bands over a relatively large volume of the Brillouin zone is expected to give rise to a number of critical points in the joint density of states with approximately the same energy separation. These nearly parallel bands are also responsible for the large, sharp structure in ϵ_2 which is found in silicon at 3.5 eV.[18] Since critical points in

TABLE VIII. Masses and curvatures for energy bands of Si and Ge.

Representation	Energy (eV) Model	Energy (eV) Experiment	Mass or Curvature Model	Mass or Curvature Experiment
		Silicon $\mathbf{k}\cdot\mathbf{p}$ expansion parameters		
$\Gamma_1=\Gamma_6^+$	−16.74	−17.0[a]	$m^*=-1.15$	
$\Gamma_{25'}^{1/2}=\Gamma_7^+$	− 0.044	− 0.044[b]	$m^*=-0.25$	− 0.25 ±0.01[b]
$\Gamma_{25'}^{3/2}=\Gamma_8^+$	0.0	0.0[c]	$A=-3.90$[d]	− 4.1 ±0.2[e]
			$B=-1.03$[d]	− 1.6 ±0.2[e]
			$\lvert C\rvert=3.79$[d]	3.3 ±0.5[e]
$\Gamma_{15}^{1/2}=\Gamma_6^-$	2.39		$m^*=0.54$	
$\Gamma_{15}^{3/2}=\Gamma_8^-$	2.43		$A=1.83$[d]	
			$B=-1.30$[d]	
			$\lvert C\rvert=2.18$[d]	
$\Gamma_{2'}=\Gamma_7^-$	3.74		$m^*=-14.0$	
$L_{2'}=L_6^-$	4.01		$m_l^*=120.0$	
			$m_t^*=0.96$	
$L_1=L_6^+$	1.77		$m_l^*=1.32$	
			$m_t^*=0.20$	
$L_1=L_6^+$	−11.07		$m_l^*=0.11$	
			$m_t^*=-2.51$	
$L_{2'}=L_6^-$	−16.58		$m_l^*=-0.33$	
			$m_t^*=2.63$	
$L_3=L_4^++L_5^+$	3.90	3.8[f]	$m_l^*=-1.45$	
			$m_t^*=-5.43$	
$=L_6^+$	3.87	3.8[f]	$m_l^*=-1.45$	
			$m_t^*=-7.47$	
$L_{3'}=L_6^-$	− 1.41	− 1.5[f]	$m_l^*=1.53$	
			$m_t^*=-0.23$	
$=L_4^-+L_5^-$	− 1.44	− 1.5[f]	$m_l^*=1.53$	
			$m_t^*=-0.21$	
$X_4=X_5$	5.63		$E'(X_5)=0.003$[g]	
			$m_l^*=-0.94$[g]	
			$\mathfrak{a}=-1.20$[g]	
			$\lvert\mathfrak{B}\rvert=0.02$[g]	
			$\lvert\mathfrak{c}\rvert=0.14$[g]	
$X_1=X_5$	1.19		$E'(X_5)=0.52$[g]	
			$m_l^*=0.96$[g]	
			$\mathfrak{a}=4.34$[g]	
			$\lvert\mathfrak{B}\rvert=0.87$[g]	
			$\lvert\mathfrak{c}\rvert=1.50$[g]	
$X_4=X_5$	− 2.55		$E'(X_5)=0.003$[g]	
			$m_l^*=1.35$[g]	
			$\mathfrak{a}=-3.66$[g]	
			$\lvert\mathfrak{B}\rvert=0.94$[g]	
			$\lvert\mathfrak{c}\rvert=2.07$[g]	
$X_1=X_5$	−14.60		$E'(X_5)=4.0$[g]	
			$m_l^*=0.35$[g]	
			$\mathfrak{a}=0.55$[g]	
			$\lvert\mathfrak{B}\rvert=0.09$[g]	
			$\lvert\mathfrak{c}\rvert=0.66$[g]	
$\Delta_1^{\min}=\Delta_6$	1.07	1.1[h]	$m_l^*=0.98$	0.97 ±0.02[i]
			$m_t^*=0.20$	0.19 ±0.01[i]
			$\delta_1=0.85$[j]	0.85 ±0.03[k]
		Germanium $\mathbf{k}\cdot\mathbf{p}$ expansion parameters		
$\Gamma_1=\Gamma^{6+}$	− 7.30	− 7.0[a]	$m^*=-1.29$	
$\Gamma_{25'}^{1/2}=\Gamma_7^+$	− 0.29	− 0.29[l]	$m^*=-0.10$	− 0.084[m]
$\Gamma_{25'}^{3/2}=\Gamma_8^+$	0.0	0.0[c]	$A=-12.78$[d]	−13.0 ±0.2[n]
			$B=-9.86$[d]	− 8.9 ±0.1[n]
			$\lvert C\rvert=9.64$[d]	10.3 ±0.2[n]
$\Gamma_{15}^{1/2}=\Gamma_6^-$	2.72	2.9[o]	$m^*=0.64$	
$\Gamma_{15}^{3/2}=\Gamma_8^-$	3.01		$A=1.24$[d]	
			$B=-1.28$[d]	
			$\lvert C\rvert=2.22$[d]	
$\Gamma_{2'}=\Gamma_7^-$	0.80	0.80[l]	$m^*=0.038$	0.040[p]

TABLE VIII (*continued*)

Representation	Energy (eV) Model	Energy (eV) Experiment	Mass or Curvature Model	Mass or Curvature Experiment
		Germanium $\mathbf{k}\cdot\mathbf{p}$ expansion parameters		
$L_{2'}=L_6^-$	3.87		$m_l^*=1.02$ $m_t^*=-1.09$	
$L_1=L_6^+$	0.66	0.664[q]	$m_l^*=1.57$ $m_t^*=0.082$	1.58 ± 0.02[i] 0.082 ± 0.002[i]
$L_1=L_6^+$	− 7.80		$m_l^*=0.33$ $m_t^*=1.85$	
$L_{2'}=L_6^-$	− 8.31		$m_l^*=1.14$ $m_t^*=-26.7$	
$L_3=L_4^++L_5^+$	4.09		$m_l^*=-1.53$ $m_t^*=0.87$	
$=L_6^+$	3.90		$m_l^*=-1.54$ $m_t^*=0.13$	
$L_{3'}=L_6^-$	− 1.41	− 1.45[r]	$m_l^*=1.31$ $m_t^*=-0.12$	
$=L_4^-+L_5^-$	− 1.61	− 1.67[r]	$m_l^*=1.31$ $m_t^*=-0.13$	
$X_4=X_5$	5.42		$E'(X_5)=0.016$[g] $m_l^*=-1.05$[g] $\mathfrak{A}=-1.27$[g] $\lvert\mathfrak{B}\rvert=0.28$[g] $\lvert\mathfrak{C}\rvert=0.24$[g]	
$X_1=X_5$	1.23		$E'(X_5)=1.09$[g] $m_l^*=0.78$[g] $\mathfrak{A}=4.59$[g] $\lvert\mathfrak{B}\rvert=5.46$[g] $\lvert\mathfrak{C}\rvert=1.89$[g]	
$X_4=X_5$	− 2.76		$E'(X_5)=0.016$[g] $m_l^*=1.06$[g] $\mathfrak{A}=-4.10$[g] $\lvert\mathfrak{B}\rvert=6.20$[g] $\lvert\mathfrak{C}\rvert=2.36$[g]	
$X_1=X_5$	− 8.64		$E'(X_5)=0.22$[g] $m_l^*=0.62$[g] $\mathfrak{A}=0.78$[g] $\lvert\mathfrak{B}\rvert=0.46$[g] $\lvert\mathfrak{C}\rvert=0.12$[g]	
$\Delta_1^{\min}=\Delta_6$	0.93		$m_l^*=0.53$ $m_t^*=0.15$ $\delta_1=0.79$[j]	

[a] References 21, 22.
[b] Reference 55.
[c] For this table the zero of energy is fixed at the top of the $\Gamma_{25'}^{3/2}=\Gamma_8^+$ valence band.
[d] The definition of the constants A, B, C is given in Eq. (59).
[e] Reference 14. The model is not sufficiently accurate to distinguish between the values in Ref. 14 and those in Refs. 15, 16, and 63. The sign of B comes from Ref. 16.
[f] Reference 19.
[g] The definition of the constants $E'(X_5)$, m_l^*, $\mathfrak{A}$, $\mathfrak{B}$, $\mathfrak{C}$ is given in Eq. (61).
[h] Reference 56.
[i] References 14, 15.
[j] The definition of δ_1 is given in Eq. (58).
[k] Reference 57.
[l] References 52–54.
[m] Reference 54. The experimental error would seem to be about 20%.
[n] Reference 14. The model is not sufficiently accurate to distinguish between the values in Ref. 14 and those in Refs. 15, 17, and 63.
[o] Reference 20.
[p] Reference 54. See also Ref. 58. The experimental error would seem to be about 15%.
[q] Reference 59.
[r] References 2, 18, 53, 59, and 65. Even if the observed structure is associated with a Λ-point transition, these values are probably accurate to about 0.1 eV.

silicon are numerous, no attempt has been made to tabulate all such points. A few of the critical points, which are related to the bands of Fig. 2, are listed in Table IX, together with the pertinent energy separations. These separations are given both with and without spin-orbit interaction. Since in silicon only a very few optical transitions are well identified, it did not seem appropriate to compare the calculated energy separations with experimental values.

Because of the rapidity of the calculation, the Fourier-expansion technique makes it feasible to explore the energy bands away from high-symmetry direc-

tions. Such an investigation was carried out by calculating the frequency dependence of the real and imaginary parts of the dielectric constant, and the results are shown in Figs. 3(a) and 3(b), respectively. The relaxation time was taken at 2×10^{-14} sec. In these figures, a comparison with the experimentally determined[18] ϵ_1 and ϵ_2 is included. No normalization procedure has been used in constructing Fig. 3(b); both the absolute magnitude and the shape of this curve are a consequence of the energy bands, themselves.

Although ϵ_2 is independent of the relaxation time τ for much of the photon energy range, there is a small τ dependence in the immediate neighborhood of the peaks. This behavior of ϵ_2 is evident upon examination of Eq. (53). This equation also indicates a more important dependence of ϵ_1 on τ. Since many approximations are associated with the introduction of a relaxation time, the calculation of ϵ_2 is considered to be more significant than that of ϵ_1.[10,11] In accordance with the dependence of ϵ_1 on τ, the relaxation time can be chosen to yield the experimental peak magnitude in ϵ_1.

From a practical point of view, the relaxation time cannot be taken too long. As τ increases, so does the number of points required to achieve a smooth curve from the Monte Carlo calculation of the dielectric constant. Fairly smooth curves, as indicated by the points in Figs. 3(a) and 3(b), were obtained with 10 000 points and $\tau=2\times10^{-14}$ sec. This value of τ corresponds to a resolution of 0.03 eV. The calculation could be carried out in a reasonable length of time on an IBM 360 computer with a speed of 1500 points/h. The results seem to indicate that better agreement with the experimental curves would result by making τ somewhat longer, perhaps $\tau\sim4\times10^{-14}$ sec.

The relatively good agreement between the calculated and experimental curves indicates that the energy bands are nearly correct in a quantitative rather than just in a qualitative sense. Discrepancies, however, do occur. For example, the leading edge in ϵ_2 at ~3.2 eV is not sharp enough and the height of the peak at 3.5 eV is too low. This behavior at the leading edge would be improved by increasing the $E(\Gamma_{15})$-$E(\Gamma_{25'})$ separation, which can be accomplished by including the next term in the Fourier expansion. Such terms would simultaneously yield better agreement with the observed band curvatures in the degenerate valence band $E(\Gamma_{25'})$. Since the experimental values for ϵ_2 below 3 eV are somewhat less certain,[67] no great effort was made to obtain good agreement in this energy region. Exciton effects have been suggested by various authors[4] to produce a sufficient intensity in the 3.5-eV peak in ϵ_2. The present calculation of the dielectric constant does not rule out this possibility, although it is not clear that a suitable refinement of the energy bands and a longer relaxation time could not reproduce the essential features of the dielectric constant, without invoking exciton effects. A longer relaxation time is also suggested by the behavior of ϵ_1 in the vicinity of 3.2 eV and of ϵ_2 in the vicinity of 4.2 eV. Since there is little experimental data for energy band gaps exceeding about 5 eV, the energy bands of Fig. 2 are less reliable far from the Fermi level. For example, in Fig. 2, the energies $E^+(L_{2'})$ and $E(L_3)$ are approximately degenerate, whereas other calculations[6,12] place $E(L_{2'})$ several electron volts above $E(L_3)$. Since there is no experimental information on this point, and since the dielectric constant is quite insensitive to the position of $E(L_{2'})$, it is not clear where this level should be placed.

The band-parameter evaluation in germanium is somewhat more tedious than in silicon, since much of the detailed experimental information in germanium pertains to energy-band separations and curvatures about the L point, rather than the Δ axis as in silicon. The expressions relating the band parameters to the experimental quantities near the L point depend on most of these parameters. Hence it is necessary to simultaneously solve a larger set of coupled equations. The procedure used in the present band-parameter determination for germanium involves the simultaneous solution of seven equations for the seven parameters $\gamma_{1,4}$ and $\gamma_{2,i}$, $i=1,\cdots,6$. A description of the method of solution is given in Appendix C. Using this method, all of the solutions for real values of these parameters are examined. Since it is not convenient to solve seven coupled nonlinear equations simultaneously, six of the seven unknowns are related by experimental measurements to the seventh parameter $\gamma_{2,2}$, which is explicitly evaluated to yield the longitudinal cyclotron effective mass for conduction electrons at the L point.[14,15] In practice, there are several solutions for $\gamma_{2,2}$ that yield the experimental value for the longitudinal cyclotron mass, and all of these solutions are examined. By requiring convergence of the Fourier series, most of these solutions are eliminated. Among the few remaining solutions, there is one solution that converges much more rapidly than the other solutions, and this is the set of parameters presented in Table VII. Solutions with less rapid convergence also presented difficulties in fitting the frequency dependence of the dielectric constant.

The remaining parameter $\gamma_{2,7}$ is determined by fitting the curvature perpendicular to the Λ axis of the lowest-conduction band at L to the observed transverse cyclotron effective-mass $m_t^*/m_0=0.082\pm0.001$.[14,15] As in the case of silicon, a numerical fitting procedure for this band parameter was found to be most convenient.

A summary of the band parameters found for germanium is given in Table VII. In this table, it is seen that the corresponding band parameters for silicon and germanium are more similar to each other for the p bands ($\gamma_{0,2},\gamma_{1,2},\gamma_{2,2},\gamma_{1,3},\gamma_{2,3},\gamma_{2,5},\gamma_{2,7}$) than they are for the s bands ($\gamma_{0,1},\gamma_{1,1},\gamma_{2,1}$) or the s-p interaction ($\gamma_{1,4},\gamma_{2,4},\gamma_{2,6}$). Not only do the s and p bands lie closer

[67] H. R. Philipp (private communication).

TABLE IX. Critical points for optical transitions in Si and Ge.

Transition	Location	Si (eV)[a]	Ge (eV)[a]
$\Gamma_{25'}-\Gamma_{2'}$	(0,0,0)	3.74{3.73, 3.77}	0.90{0.80, 1.09}
$\Gamma_{25'}-\Gamma_{15}$	(0,0,0)	2.43{2.39, 2.43, 2.47}	2.84{2.55, 2.84, 3.13}
$L_{3'}-L_1$	$(\pi/a)(0.5,0.5,0.5)$	3.20{3.18, 3.21}	2.18{2.08, 2.27}
$\Lambda_3-\Lambda_1$	$(\pi/a)(\eta,\eta,\eta)$	3.22{3.20, 3.23} $\eta=0.3$	2.17{2.07, 2.26} $\eta=0.4$
			2.22{2.11, 2.32} $\eta=0.2$
$L_{3'}-L_3$	$(\pi/a)(0.5,0.5,0.5)$	5.30{5.27, 5.30, 5.33}	5.51{5.32, 5.51, 5.70}
$L_{3'}-L_{2'}$	$(\pi/a)(0.5,0.5,0.5)$	5.44{5.42, 5.45}	5.38{5.29, 5.48}
$\Delta_5-\Delta_{2'}$	$(\pi/a)(\eta,0,0)$	4.53{4.527, 4.533} $\eta=0.4$	4.92{4.90, 4.94} $\eta=0.6$
$\Sigma_2-\Sigma_3$	$(\pi/a)(\eta,\eta,0)$	4.43 $\eta=0.6$	4.12 $\eta=0.6$
$L-U$ axis	$(\pi/a)(0.8,0.25,0.25)$	4.33	4.14

[a] Spin-orbit splittings are indicated by brackets where they occur.

to each other in germanium, but also the d bands are closer to the Fermi level. Therefore, even though there are a larger number of well-identified optical transitions in germanium, and the band-parameter determination can be made with more confidence, the calculated energy bands provide a quantitative description of the bands for a smaller energy range away from the Fermi level than for the case of silicon. Inspection of Table VII shows that the band parameters of silicon and germanium converge with approximately the same rapidity. Therefore, the discussion given for the uncertainties in the silicon band parameters of this table applies equally well to those of germanium.

Using the band parameters for germanium given in Table VII, band curvatures including the effect of spin-orbit interaction have been calculated at the same high-symmetry points as for silicon. The effective masses and band curvatures are summarized in Table VIII, and wherever possible a comparison with experimental values is included. This table also compares the various effective mass quantities in silicon and germanium. In general, the agreement between the observed and calculated values is better for germanium than for silicon, since the band-parameter determination in germanium depends upon more firmly established data than in silicon. In fact, by including only terms to next-nearest-neighbor interactions in the Fourier series, most of the experimental data for germanium is well satisfied. Because of the larger spin-orbit interaction in germanium, this interaction has a more important effect on the curvature of the degenerate energy bands at Γ and L. At the X point, the slopes $E'(X_5)$ of the levels derived from the degenerate X_4 bands are considerably larger in germanium than in silicon.

The energy bands in germanium along certain high-

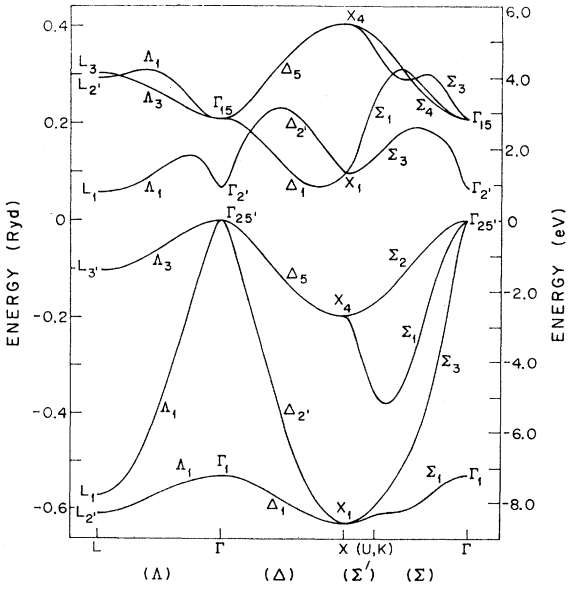

FIG. 4. Energy versus dimensionless wave vector for a few high-symmetry directions in germanium. Spin-orbit interaction has been neglected.

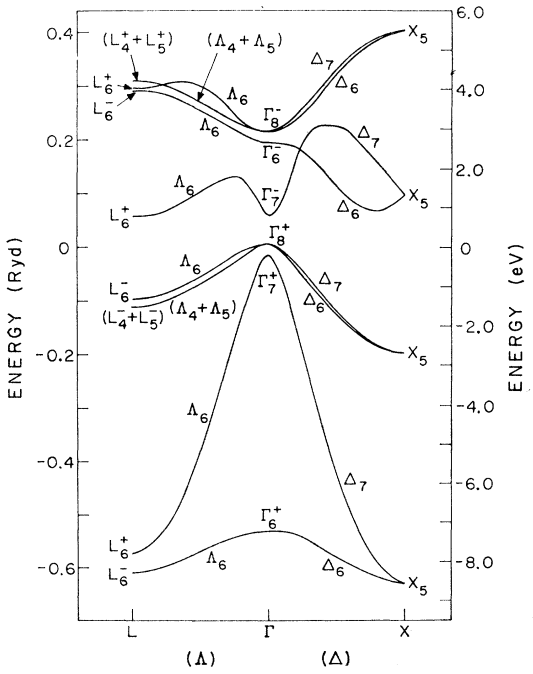

FIG. 5. Energy versus dimensionless wave vector for a few high-symmetry directions in germanium. Spin-orbit interaction has been included and the bands are labeled by the double group representations.

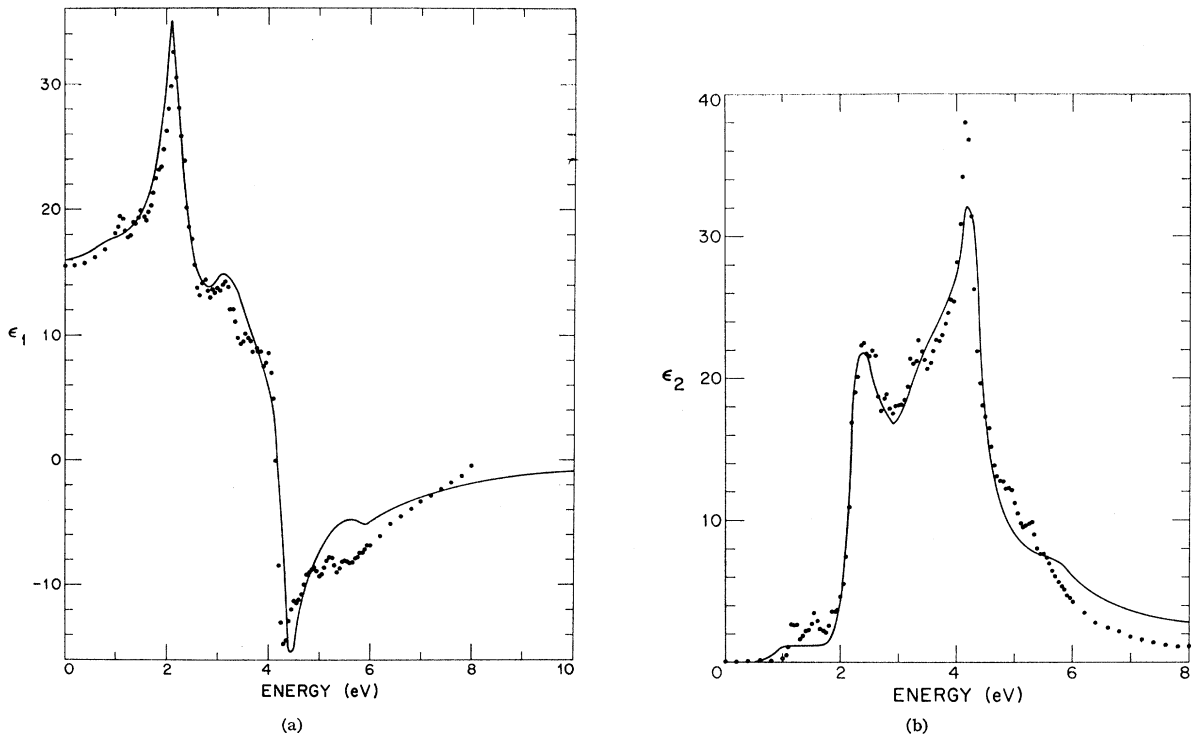

FIG. 6. Frequency dependence of the real (ϵ_1) and imaginary (ϵ_2) parts of the dielectric constant for germanium. The solid curves represent Philipp's Kramers-Kronig analysis of experimental reflectivity data (see Ref. 70) while the dots are calculated by a Monte Carlo procedure using 10 000 points and $\tau=2\times10^{-14}$ sec.

symmetry directions are shown in Fig. 4 for the case where the spin-orbit interaction is ignored and in Fig. 5 where this interaction is treated explicitly. In silicon, the spin-orbit interaction is so small that the corresponding two figures would be nearly coincident. With only one spin-orbit band parameter, equal spin-orbit splittings of $\Delta=0.29$ eV are found for the degenerate $E(\Gamma_{15})$ and $E(\Gamma_{25'})$ levels. The spin-orbit splittings of degenerate bands at other high-symmetry points are smaller. A summary of calculated spin-orbit splittings for germanium at various points in the Brillouin zone is given in Table VIII and, wherever possible, a comparison is made with observed splittings. With improved resolution of optical structure, these spin-orbit splittings can be utilized in the identification of optical structure with interband transitions at specific points in the Brillouin zone and between specific energy bands. As in the case of silicon, these energy bands are in qualitative agreement with other band calculations.[6,12] The energy-band separations for several of the bands shown in Figs. 4 and 5 are approximately constant over relatively large volumes of the Brillouin zone, thereby resulting in a fairly large number of critical points in the joint density of states. As in silicon, these critical points can occur at general points in the Brillouin zone. Critical points along afew of the high-symmetry axes are listed in Table IX, along with the corresponding energy differences. The results are presented both with and without spin-orbit interaction. Since the $E(\Lambda_3)$ and $E(\Lambda_1)$ levels are almost parallel along much of the Λ axis, several critical points are found at $\sim(\pi/a)(0.2,0.2,0.2)$, $\sim(\pi/a)(0.4,0.4,0.4)$ as well as at $L=(\pi/a)(0.5,0.5,0.5)$. The spin-orbit splitting at $(\pi/a)(0.2,0.2,0.2)$ is 0.21 eV, while for the other two critical points the splitting is 0.19 eV. There is some experimental evidence supporting multiple critical points along the Λ axis, although their number and location have not been well established. Recently, Potter's measurements of the optical constants of germanium[68] have revealed two sets of optical structures in the vicinity of 2 eV, separated by about these spin-orbit splittings. Piezoelectroreflectance studies by Cardona and Pollak indicate that the $(\pi/a)(0.2,0.2,0.2)$ critical point contributes strongly to the observed structure.[69]

The frequency dependence of the real and imaginary parts of the dielectric constant for germanium based on the energy bands of Fig. 4 is given in Figs. 6(a) and 6(b), respectively. In these figures, a comparison is also made with the experimental determination of these quantities.[70] The calculated points are based on simpler energy

[68] R. F. Potter, Phys. Rev. **150**, 562 (1966).
[69] M. Cardona and F. H. Pollak, Bull. Am. Phys. Soc. **12**, 101 (1967).
[70] The Kramers-Kronig analysis carried out by Dr. H. R. Philipp was based on reflectivity measurements by T. M. Donovan, E. J. Ashley, and H. E. Bennett [J. Opt. Soc. Am. **53**, 1403 (1963)].

bands, which neglect spin-orbit interaction. The relaxation time was taken as $\tau=2\times10^{-14}$ sec, which gives results for the extremal values of ϵ_1 that are consistent with the experimental data, as shown in Fig. 6(a). The Monte Carlo integration procedure was carried out for 10 000 points in $\mathbf{k}$ space. In the photon energy range $2<\hbar\omega<5$ eV, excellent agreement is obtained between the calculated and experimental curves. Below about 2 eV, the agreement is not as good for two reasons. On one hand, the experimental data in this region is less certain,[67] and on the other hand, since the contribution in this photon energy range occurs from a small volume around Γ, a very large number of Monte Carlo points are needed to obtain a smooth curve in ϵ_2. Above about 5 eV, the agreement is also not as good. In this energy range, there are not so many experimental data available, and the d bands, which have not been explicitly treated, become important.[18]

With the increasing availability of reliable optical data, it has become fashionable to identify certain optical structures with interband transitions.[4] The excellent agreement illustrated in Figs. 6(a) and (6b) for the energy range $2<\hbar\omega<5$ eV indicates that the calculated energy bands provide a good description of the the actual energy bands in germanium. Therefore, it is possible to investigate the critical points that are associated with the various optical structures. For example, the sharp, leading edge in ϵ_2 at 2.1 eV is closely associated with the various $\Lambda_3\rightarrow\Lambda_1$ transitions along the Λ axis, and including the $E(L_{3'})\rightarrow E(L_1)$ transition at the L point. This assignment has also been made by numerous other authors.[4] The onset of the second rise in ϵ_2 at 2.9 eV is closely identified with the $E(\Gamma_{25'})\rightarrow E(\Gamma_{15})$ transition, and this also is in agreement with the results of other authors.[6] However, in this dielectric-constant calculation, the identification of the sharp peak in ϵ_2 at 4.2 eV is not found to be particularly closely related to any single transition such as the $E^-(X_4)\rightarrow E^+(X_1)$ transition.[4] In fact, in order to obtain this sharp peak at the observed photon energy, the $E^+(X_1)-E^-(X_4)$ separation was taken at 4.0 eV, which corresponds to the beginning of the sharp rise in ϵ_2. Since pairs of energy bands, separated by about 4.2 eV, are nearly parallel over a large volume of the Brillouin zone, there are numerous critical points at about this energy. For example, in Table IX, critical points are listed along the Σ axis with a 4.12-eV separation and along the L-U axis with a 4.14-eV separation. Experience gained from this dielectric-constant calculation indicates that the identification of optical structure with a particular critical point is sometimes dangerous. Although some structures are identified with a small volume of the Brillouin zone, others involve large volumes. The availability of a band model which is amenable to the rapid calculation of experimental quantities should prove useful in the identification of optical structures with specific critical points.

In this paper it is seen that a one-electron effective-mass Hamiltonian can be used to describe the observed optical properties of silicon and germanium. For energies sufficiently small so that the effect of the d bands is not important, it would appear that any small discrepancies which exist between the observed and calculated dielectric constants could probably be corrected by including higher-order terms in the Fourier expansion. However, as the experimental data become more and more precise, it is likely that discrepancies will arise which cannot be handled by a one-electron Hamiltonian, no matter how many Fourier terms are included. Certain many-body effects are, in fact, included in the one-electron Hamiltonian, because of the experimental determination of the energy-band parameters. However, the origin of these contributions is not examined in any detail; hence, contributions from the exchange, correlation, electron-phonon interaction, etc. are not distinguished from one another. From a many-body point of view, the term which has been retained is the first term in the expansion of the Landau theory of the Fermi liquid.[71]

In metals, there is considerable discussion about the effect of electron-phonon interaction on the one-electron energy bands.[72] If this interaction is large, it might be necessary to include many terms in the Fourier expansion. An alternate and more rapidly convergent procedure would be to Fourier expand the electron-phonon interaction directly and then to solve the coupled problem for the energy eigenvalues. The general application of the Fourier-expansion technique to treating the lattice-vibration problem and the electron-phonon interaction is presented elsewhere.[46]

ACKNOWLEDGMENTS

The authors are grateful to D. Buss for help with the dielectric-constant calculation. We would like to thank Dr. H. R. Philipp for kindly supplying his most recent Kramers-Kronig analysis of reflectivity data in silicon and germanium. We would also like to acknowledge stimulating discussions with Dr. P. N. Argyres, Dr. J. Feinleib, Dr. S. H. Groves, Dr. F. Herman, Dr. E. O. Kane, Dr. P. L. Kelley, Dr. W. H. Kleiner, Dr. M. Maltz, Dr. J. G. Mavroides, Dr. H. J. Zeiger, Professor B. Lax, Professor G. W. Pratt, and Professor L. M. Roth, as well as numerous other colleagues.

APPENDIX A: CONTRIBUTIONS TO THE EFFECTIVE-MASS HAMILTONIAN FROM THIRD AND FOURTH NEIGHBORS

As more experimental information becomes available for silicon and germanium, a more precise determination of the energy bands for these materials can be

[71] P. Nozières, *Theory of Interacting Fermi Systems* (W. A. Benjamin, Inc., New York, 1964).

[72] W. A. Harrison, *Pseudopotentials in the Theory of Metals* (W. A. Benjamin, Inc., New York, 1966), p. 125.

carried out by including more distant-neighbor interactions in the effective-mass Hamiltonian. In Table X, a summary is given for various neighbor distances in the diamond lattice, and the number of band parameters or Fourier coefficients associated with each neighbor is also included. Since the third-neighbor distance is relatively close to the second-neighbor distance, third-neighbor contributions to the Fourier expansion might be expected to be of some importance in constructing the energy bands in these materials. In order to evaluate seven band parameters associated with third-neighbor interactions ($\alpha=3$), seven additional pieces of experimental information need to be introduced.

From the symmetry properties of the diamond lattice, the additional terms in the effective-mass Hamiltonian arising from third-neighbor interactions are of the form $h_1(\mathbf{k})$ and $g_1(\mathbf{k})$ and can be written as

$$\begin{aligned}h_1^{(3)}(\mathbf{k})=&\gamma_{3,1}[C(3,\mathbf{k};\Gamma_1)+12]S(s,\Gamma_1)\\&+\gamma_{3,2}[C(3,\mathbf{k};\Gamma_1)+12]S(p,\Gamma_1)\\&+\{\gamma_{3,3a}\mathbf{C}(3,\mathbf{k};\Gamma_{25'}a)+\gamma_{3,3b}\mathbf{C}(3,\mathbf{k};\Gamma_{25'}b)\}\cdot\mathbf{S}(p,\Gamma_{25'})\\&+\{\gamma_{3,4a}\mathbf{C}(3,\mathbf{k};\Gamma_{15}a)+\gamma_{3,4b}\mathbf{C}(3,\mathbf{k};\Gamma_{15}b)\}\cdot\mathbf{S}(sp,\Gamma_{15})\\&+\gamma_{3,5}\mathbf{C}^*(3,\mathbf{k};\Gamma_{12})\cdot\mathbf{S}(p,\Gamma_{12}),\end{aligned}\tag{A1}$$

and

$$g_1^{(3)}(\mathbf{k})=h_1^{(3)}[\mathbf{k}+(\pi/a)(1,1,1)].\tag{A2}$$

These terms merely add to the $h_1(\mathbf{k})$ and $g_1(\mathbf{k})$ functions given by Eqs. (10) and (12), respectively. In order to maintain the top of the valence band $E(\Gamma_{25'})$ at the zero of energy, a constant energy $h_0^{(3)}$

$$h_0^{(3)}=-12\gamma_{3,1}S(s,\Gamma_1)-12\gamma_{3,2}S(p,\Gamma_1)\tag{A3}$$

must be supplied, and this is added to $h_0(\mathbf{k})$ in Eq. (9).

In a similar way, the terms arising from fourth-neighbor interactions are all of the form $h_0(\mathbf{k})$ and are explicitly written as

$$\begin{aligned}h_0^{(4)}(\mathbf{k})=&\gamma_{4,1}C(4,\mathbf{k};\Gamma_1)S(s,\Gamma_1)+\gamma_{4,2}C(4,\mathbf{k};\Gamma_1)S(p,\Gamma_1)\\&+\gamma_{4,4}\mathbf{C}(4,\mathbf{k};\Gamma_{15})\cdot\mathbf{S}(sp,\Gamma_{15})\\&+\gamma_{4,5}\mathbf{C}^*(4,\mathbf{k};\Gamma_{12})\cdot\mathbf{S}(p,\Gamma_{12}),\end{aligned}\tag{A4}$$

so that $h_0^{(4)}(\mathbf{k})$ is the next term in the expansion of $h_0(\mathbf{k})$ given by Eq. (9). The additional band parameters $\gamma_{\alpha,\beta}$ of Eqs. (A1) and (A4) which are introduced with third- and fourth-neighbor interactions are listed in Table XI, which is an extension of Table I, given in the main body of the paper. A band-parameter identification is made only with the coefficients used by Dresselhaus,[46] since no corresponding terms occur in the treatment by Slater and Koster.[33] In the band-parameter notation $\gamma_{\alpha,\beta}$, α denotes the αth neighbor, whereas β labels the various Fourier coefficients corresponding to each α. A particular β index describes a symmetry type Γ_i which arises from coupling bands with symmetries Γ_j and Γ_k, so that the symmetry types involved in $\gamma_{3,1}$ are the same as in $\gamma_{0,1}$, $\gamma_{1,1}$, and in $\gamma_{2,1}$. Now, for an arbitrary lattice point $a(l,m,n)$, $|l|\neq|m|\neq|n|$, there are as many symmetrized Fourier functions $C(\alpha,\mathbf{k};\Gamma_\beta)$ as the dimensionality of the representation Γ_β. For example, the band parameter $\gamma_{\alpha,3}$ refers to a three-dimensional representation $\Gamma_{25'}$, and there can be as many as three distinct symmetrized Fourier functions and associated Fourier coefficients. For the lattice point $\frac{1}{2}a(3,1,1)$, $m=n$, and only two distinct functions occur; and the pertinent band parameters are labeled $\gamma_{3,3a}$ and $\gamma_{3,3b}$. Table XII lists the symmetrized Fourier functions which occur for third-neighbor interactions, while Table XIII lists the corresponding functions for fourth-neighbor interactions. The basis matrices which enter Eqs. (A1)–(A4) are listed in Table III.

The energy levels at $\mathbf{k}=0$ still depend on only a few band parameters:

$$\begin{aligned}E(\Gamma_1)&=\gamma_{0,1}\\E(\Gamma_{2'})&=\gamma_{0,1}-8\gamma_{1,1}-24\gamma_{3,1}\\E(\Gamma_{15})&=\gamma_{0,2}\\E(\Gamma_{25'})&=\gamma_{0,2}-8\gamma_{1,2}-24\gamma_{3,2}.\end{aligned}\tag{A5}$$

Since the energy levels at the Γ point do not depend on the band parameters for second-neighbor interactions $\alpha=2$, the terms for $\alpha=3$, which occur with rather large

TABLE X. Number of band parameters for various neighbor distances in diamond lattice.

Neighbor	Number of band parameters	Coordinates	Distance
0	2	$a(0,0,0)$	$a0.0$
1	4	$\frac{1}{2}a(1,1,1)$	$a0.866$
2	7	$a(1,1,0)$	$a1.414$
3	7	$\frac{1}{2}a(3,1,1)$	$a1.66$
4	4	$a(2,0,0)$	$a2.0$
5	7	$\frac{1}{2}a(3,3,1)$	$a2.18$
6	10	$a(2,1,1)$	$a2.45$
7	4	$\frac{1}{2}a(3,3,3)$	$a2.60$

TABLE XI. Band-parameter notation for third and fourth neighbors.

This paper	D[a]
$\gamma_{3,1}$	$2\alpha[(\frac{3}{2}\,\frac{1}{2}\,\frac{1}{2}),\Gamma_1;\ \Gamma_1\leftrightarrow\Gamma_1]$
$\gamma_{3,2}$	$2\alpha[(\frac{3}{2}\,\frac{1}{2}\,\frac{1}{2}),\Gamma_1;\ \Gamma_{15}\leftrightarrow\Gamma_{15}]$
$\gamma_{3,3a}$	$2\alpha[(\frac{3}{2}\,\frac{1}{2}\,\frac{1}{2}),\Gamma_{25'}a;\ \Gamma_{15}\leftrightarrow\Gamma_{15}]$
$\gamma_{3,3b}$	$2\alpha[(\frac{3}{2}\,\frac{1}{2}\,\frac{1}{2}),\Gamma_{25'}b;\ \Gamma_{15}\leftrightarrow\Gamma_{15}]$
$\gamma_{3,4a}$	$2\alpha[(\frac{3}{2}\,\frac{1}{2}\,\frac{1}{2}),\ \Gamma_{15}a;\ \Gamma_1\leftrightarrow\Gamma_{15}]$
$\gamma_{3,4b}$	$2\alpha[(\frac{3}{2}\,\frac{1}{2}\,\frac{1}{2}),\ \Gamma_{15}b;\ \Gamma_1\leftrightarrow\Gamma_{15}]$
$\gamma_{3,5}$	$2\alpha[(\frac{3}{2}\,\frac{1}{2}\,\frac{1}{2}),\ \Gamma_{12};\ \Gamma_{15}\leftrightarrow\Gamma_{15}]$
$\gamma_{4,1}$	$8\alpha[(200),\ \Gamma_1;\ \Gamma_1\leftrightarrow\Gamma_1]$
$\gamma_{4,2}$	$8\alpha[(200),\ \Gamma_1;\ \Gamma_{15}\leftrightarrow\Gamma_{15}]$
$\gamma_{4,4}$	$8\alpha[(200),\ \Gamma_{15};\ \Gamma_1\leftrightarrow\Gamma_{15}]$
$\gamma_{4,5}$	$8\alpha[(200),\ \Gamma_{12};\ \Gamma_{15}\leftrightarrow\Gamma_{15}]$

[a] See Ref. 46. Because of the choice of zero of energy, the $\gamma_{0,1}$ and $\gamma_{0,2}$ of Table I are re-identified with the band parameters of Ref. 46 according to the relations

$$\gamma_{0,1}=24\alpha((000),\Gamma_1;\ \Gamma_1\leftrightarrow\Gamma_1)+4\gamma_{1,1}+6\gamma_{2,1}+12\gamma_{3,1}+3\gamma_{4,1}$$
$$\gamma_{0,2}=24\alpha((000),\Gamma_1;\ \Gamma_{15}\leftrightarrow\Gamma_{15})+4\gamma_{1,2}+6\gamma_{2,2}+12\gamma_{3,2}+3\gamma_{4,2},$$

while the definitions for the band parameters $\gamma_{1,\beta}$ and $\gamma_{2,\beta}$ are unchanged.

TABLE XII. Symmetrized Fourier functions for third-neighbor interactions in a diamond lattice.[a]

	$3\xi+\eta+\zeta$	$\xi+3\eta+\zeta$	$\xi+\eta+3\zeta$	$3\xi-\eta-\zeta$	$-\xi+3\eta-\zeta$	$-\xi-\eta+3\zeta$	$-3\xi-\eta+\zeta$	$\xi-3\eta-\zeta$	$-\xi+\eta-3\zeta$	$-3\xi+\eta-\zeta$	$-\xi-3\eta+\zeta$	$\xi-\eta-3\zeta$
$C(3,\mathbf{k};\Gamma_1)+12$	C	C	C	C	C	C	C	C	C	C	C	C
$C(3,\mathbf{k};\Gamma_{2'})$	S	S	S	S	S	S	S	S	S	S	S	S
$C_1(3,\mathbf{k};\Gamma_{12})$	C	ωC	$\omega^2 C$	C	ωC	$\omega^2 C$	C	ωC	$\omega^2 C$	C	ωC	$\omega^2 C$
$C_1(3,\mathbf{k};\Gamma_{12'})$	S	ωS	$\omega^2 S$	S	ωS	$\omega^2 S$	S	ωS	$\omega^2 S$	S	ωS	$\omega^2 S$
$C_x(3,\mathbf{k};\Gamma_{25'}a)$	C			C			$-C$			$-C$		
$C_x(3,\mathbf{k};\Gamma_{15}a)$	S			S			$-S$			$-S$		
$C_x(3,\mathbf{k};\Gamma_{25'}b)$		C	C		$-C$	$-C$		C	$-C$		$-C$	C
$C_x(3,\mathbf{k};\Gamma_{15}b)$		S	S		$-S$	$-S$		S	$-S$		$-S$	S
$C_x(3,\mathbf{k};\Gamma_{15'})$		$-C$	C		C	$-C$		$-C$	$-C$		C	C
$C_x(3,\mathbf{k};\Gamma_{25})$		$-S$	S		S	$-S$		$-S$	$-S$		S	S

[a] In this table $(\xi,\eta,\zeta)=\frac{1}{2}a(k_x,k_y,k_z)$ and $\omega=e^{2\pi i/3}$. A C indicates that the cosine of the argument at the top of the column is taken whereas an S indicates the sine. The $C_2(3,\mathbf{k};\Gamma_{12})$ and $C_2(3,\mathbf{k};\Gamma_{12'})$ entries are the complex conjugates of the entries given. The C_y and C_z entries are obtained by cyclic permutations of k_x, k_y, and k_z.

TABLE XIII. Symmetrized Fourier functions for fourth-neighbor interactions in a diamond lattice.[a]

$$C(4,\mathbf{k};\Gamma_1)=-3+\cos 2ak_x+\cos 2ak_y+\cos 2ak_z$$
$$C_1(4,\mathbf{k};\Gamma_{12})=\cos 2ak_x+\omega\cos 2ak_y+\omega^2\cos 2ak_z$$
$$C_2(4,\mathbf{k};\Gamma_{12})=\cos 2ak_x+\omega^2\cos 2ak_y+\omega\cos 2ak_z$$
$$C_x(4,\mathbf{k};\Gamma_{15})=\sin 2ak_x$$
$$C_y(4,\mathbf{k};\Gamma_{15})=\sin 2ak_y$$
$$C_z(4,\mathbf{k};\Gamma_{15})=\sin 2ak_z$$

[a] Where $\omega=e^{2\pi i/3}$

coefficients, can lead to significant corrections to these energy levels. It is of interest that terms in $\alpha=4$ do not contribute to the energy levels at Γ.

On the other hand, the terms in $\alpha\geqslant 3$ are of less importance in determining the energy levels at other points in the Brillouin zone. In particular, the energy levels at the X point to terms in $\alpha=4$ are given by

$$E^{\pm}(X_4)=\gamma_{0,2}-4\gamma_{1,2}-8\gamma_{2,2}-4\gamma_{2,5}-12\gamma_{3,2}\pm 4[\gamma_{1,3}+\gamma_{3,3a}-2\gamma_{3,3b}], \quad \text{(A6)}$$

$$E^{\pm}(X_1)=\tfrac{1}{2}[(\chi_{11}+\chi_{22})\pm((\chi_{11}-\chi_{22})^2+4|\chi_{12}|^2)^{1/2}], \quad \text{(A7)}$$

where

$$\chi_{11}=\gamma_{0,1}-4\gamma_{1,1}-8\gamma_{2,1}-12\gamma_{3,1},$$
$$\chi_{22}=\gamma_{0,2}-4\gamma_{1,2}-8\gamma_{2,2}+8\gamma_{2,5}-12\gamma_{3,2}, \quad \text{(A8)}$$
$$\chi_{12}=4i[\gamma_{1,4}-\gamma_{3,4a}+2\gamma_{3,4b}].$$

In Eqs. (A6)–(A8) the band parameters $\gamma_{3,1}$ and $\gamma_{3,2}$ enter in the same combination as in Eq. (A5) for the Γ point, and, therefore, these terms are easily eliminated from the equations for $E^{\pm}(X_4)$ and $E^{\pm}(X_1)$. Furthermore, since the parameters $\gamma_{3,3a}$, $\gamma_{3,3b}$, $\gamma_{3,4a}$, and $\gamma_{3,4b}$ enter with small coefficients, these parameters are not expected to be very important for the X-point energy levels. It is of interest that these energy levels do not depend on terms in $\alpha=4$.

Although the energy levels at the L point depend on a larger number of band parameters, even here many of these parameters enter in the same combinations as at the Γ and X points. The doubly degenerate levels $E^{\pm}(L_3)$ are given by

$$E^{\pm}(L_3)=\gamma_{0,2}-4\gamma_{1,2}-6\gamma_{2,2}+2\gamma_{2,3}-12\gamma_{3,2}-6\gamma_{4,2}\pm 2(\gamma_{1,2}+\gamma_{1,3}-3\gamma_{3,2}-\gamma_{3,3a}+2\gamma_{3,3b}), \quad \text{(A9)}$$

while the nondegenerate levels $E^{\pm}(L_1)$ and $E^{\pm}(L_{2'})$ are given by Eq. (31), where the quantities $A(L_i)$, $B(L_i)$, and $C(L_i)$, which contain band parameters for $\alpha\leqslant 2$, are replaced by $A^{(4)}(L_i)$, $B^{(4)}(L_i)$, and $C^{(4)}(L_i)$ which include terms to $\alpha\leqslant 4$:

$$A^{(4)}(L_1)=A(L_1)-6\gamma_{3,1}-6\gamma_{4,1},$$
$$B^{(4)}(L_1)=B(L_1)-18\gamma_{3,2}+4(\gamma_{3,3a}-2\gamma_{3,3b})-6\gamma_{4,2}, \quad \text{(A10)}$$
$$C^{(4)}(L_1)=C(L_1)-2(3)^{1/2}(\gamma_{3,4a}-2\gamma_{3,4b}),$$

$$A^{(4)}(L_{2'})=A(L_{2'})-18\gamma_{3,1}-6\gamma_{4,1},$$
$$B^{(4)}(L_{2'})=B(L_{2'})-6\gamma_{3,2}-4(\gamma_{3,3a}-2\gamma_{3,3b})-6\gamma_{4,2}, \quad \text{(A11)}$$
$$C^{(4)}(L_{2'})=C(L_{2'})+2(3)^{1/2}(\gamma_{3,4a}-2\gamma_{3,4b}).$$

In addition to these energy levels, the band-parameter determination involves certain band curvatures. These band curvatures at the Γ point are particularly sensitive to the higher-Fourier coefficients. Explicit expressions for

the nondegenerate bands $E(\Gamma_1;\mathbf{k})$ and $E(\Gamma_{2'};\mathbf{k})$ to terms in $\alpha\lesssim 4$ are

$$E(\Gamma_1,\mathbf{k})=\gamma_{0,1}+(ak)^2\{-\tfrac{1}{2}\gamma_{1,1}-2\gamma_{2,1}-(11/2)\gamma_{3,1}-2\gamma_{4,1}+(2\gamma_{1,4}+4\gamma_{2,4}+6\gamma_{3,4a}+4\gamma_{3,4b}+2\gamma_{4,4})^2[E(\Gamma_1)-E(E_{15})]^{-1}\}, \quad \text{(A12)}$$

$$E(\Gamma_{2'},\mathbf{k})=\gamma_{0,1}-8\gamma_{1,1}-24\gamma_{3,1}+(ak)^2\{\tfrac{1}{2}\gamma_{1,1}-2\gamma_{2,1}+(11/2)\gamma_{3,1}-2\gamma_{4,1}+(-2\gamma_{1,4}+4\gamma_{2,4}-6\gamma_{3,4a}-4\gamma_{3,4b}+2\gamma_{4,4})^2[E(\Gamma_{2'})-E(\Gamma_{25'})]^{-1}\}, \quad \text{(A13)}$$

while the effective-mass parameters for the degenerate bands $E(\Gamma_{15})$ and $E(\Gamma_{25'})$ are given by

$$L(\Gamma_{15})=-\tfrac{1}{2}\gamma_{1,2}-2\gamma_{2,2}+2\gamma_{2,5}-(11/2)\gamma_{3,2}-8\gamma_{3,5}-2\gamma_{4,2}-4\gamma_{4,5}+(2\gamma_{1,4}+4\gamma_{2,4}+6\gamma_{3,4a}+4\gamma_{3,4b}+2\gamma_{4,4})^2[E(\Gamma_{15})-E(\Gamma_1)]^{-1}, \quad \text{(A14)}$$

$$M(\Gamma_{15})=-\tfrac{1}{2}\gamma_{1,2}-2\gamma_{2,2}-\gamma_{2,5}-(11/2)\gamma_{3,2}+4\gamma_{3,5}-2\gamma_{4,2}+2\gamma_{4,5}+(2\gamma_{1,3}-6\gamma_{3,3a}-4\gamma_{3,3b})^2[E(\Gamma_{15})-E(\Gamma_{25'})]^{-1}, \quad \text{(A15)}$$

$$Q(\Gamma_{15})=-\gamma_{1,2}-4\gamma_{2,2}+\gamma_{2,5}+\gamma_{1,3}+2\gamma_{2,3}-11\gamma_{3,2}-4\gamma_{3,5}-4\gamma_{4,2}-2\gamma_{4,5}+\gamma_{3,3a}+6\gamma_{3,3b}, \quad \text{(A16)}$$

for the degenerate conduction band, and by

$$L(\Gamma_{25'})=\tfrac{1}{2}\gamma_{1,2}-2\gamma_{2,2}+2\gamma_{2,5}+(11/2)\gamma_{3,2}+8\gamma_{3,5}-2\gamma_{4,2}-4\gamma_{4,5}+(-2\gamma_{1,4}+4\gamma_{2,4}-6\gamma_{3,4a}-4\gamma_{3,4b}+2\gamma_{4,4})^2[E(\Gamma_{25'})-E(\Gamma_{2'})]^{-1}, \quad \text{(A17)}$$

$$M(\Gamma_{25'})=\tfrac{1}{2}\gamma_{1,2}-2\gamma_{2,2}-\gamma_{2,5}+(11/2)\gamma_{3,2}-4\gamma_{3,5}-2\gamma_{4,2}+2\gamma_{4,5}+(-2\gamma_{1,3}+6\gamma_{3,3a}+4\gamma_{3,3b})^2[E(\Gamma_{25'})-E(\Gamma_{15})]^{-1}, \quad \text{(A18)}$$

$$Q(\Gamma_{25'})=\gamma_{1,2}-4\gamma_{2,2}+\gamma_{2,5}-\gamma_{1,3}+2\gamma_{2,3}+11\gamma_{3,2}+4\gamma_{3,5}-4\gamma_{4,2}-2\gamma_{4,5}-\gamma_{3,3a}-6\gamma_{3,3b}, \quad \text{(A19)}$$

for the degenerate valence band. Higher-Fourier coefficients are relatively more important in these effective-mass formulas, because these higher-order band parameters enter with larger coefficients and in different combinations than occur in the energy levels themselves.

APPENDIX B: SOLUTION OF COUPLED EQUATIONS IN SILICON

For silicon, the four variables $\gamma_{1,4}$, $\gamma_{2,4}$, $\gamma_{2,1}$, and $\gamma_{2,25}=\gamma_{2,2}-\gamma_{2,5}$ are evaluated from solution of four coupled equations. The four pieces of experimental data that are involved are the energy and location of the conduction-band minimum $E(\Delta_1^{\min})$, the longitudinal cyclotron effective-mass at $\Delta_1^{\min}$ and the effective-mass quantity L of the $E(\Gamma_{25'})$ valence band. Since the coupled equations are written in terms of the energy and derivatives of the $E^+(X_1)$ band at the X point, it is convenient to relate these quantities to the observables $E(\Delta_1^{\min})$, m_l^* and δ_1 by the relations

$$E^+(X_1)=E^+(\Delta_1^{\min})+\frac{\hbar^2\pi^2}{2m_l^*a^2}(1-\delta_1)^2, \quad \text{(B1)}$$

$$\frac{\partial E^+(X_1)}{\partial(ak_x)}=\frac{\hbar^2\pi}{m_l^*a^2}(1-\delta_1), \quad \text{(B2)}$$

$$\frac{\partial^2 E^+(X_1)}{\partial(ak_x)^2}=\frac{\hbar^2}{m_l^*a^2}. \quad \text{(B3)}$$

Optical measurement of the indirect gap in silicon[56] yields a room-temperature value $E(\Delta_1^{\min})=1.114$ eV, while cyclotron-resonance experiments on the electrons[14,15] provide a value $m_l^*/m_0=0.97\pm0.02$ at $\Delta_1^{\min}$. By direct computation of the curvature of $E^+(\Delta_1^{\min})$ (see Table VIII) about the energy minimum and about the X point, it is found that the band curvatures at these two points differ by about 2%, which is within the experimental error in the effective-mass measurement of m_l^*.[14,15] Analysis of the spacial variation of the electron wave function for donor-impurity states[57] has yielded the location of the conduction-band minima on the Δ axis at $ak=\pi\delta_1$, where $\delta_1=0.85\pm0.03$.

The four coupled equations which are to be evaluated are conveniently written in terms of the four variables

$$\begin{aligned} a&=[\gamma_{0,1}-4_{1,1}-E^+(X_1)]-8\gamma_{2,1},\\ b&=[4\gamma_{1,2}-E^+(X_1)]-8(\gamma_{2,2}-\gamma_{2,5}),\\ d&=4\gamma_{1,4},\\ f&=4\gamma_{2,4}, \end{aligned} \quad \text{(B4)}$$

in which the quantities in the square brackets are constants which have already been evaluated. The first of the four coupled equations is obtained by rewriting Eq. (17) for $E^+(X_1)$ in terms of the variables of Eq. (B4), yielding

$$ab=d^2. \quad \text{(B5)}$$

The second equation is found by differentiating Eq. (15) and then rewriting it in the form

$$[\partial E^+(X_1)/\partial(ak_x)](a+b)=-2(a\gamma_{1,2}+b\gamma_{1,1})+2df. \quad \text{(B6)}$$

The third equation arises from taking a second derivative of Eq. (15), and is written in the form

$$aA+bB+C=-\tfrac{1}{2}d^2-2f^2, \tag{B7}$$

in which the coefficients A, B, and C are treated as constants and are written as

$$\begin{aligned} A&=[\partial^2E^+(X_1)/\partial(ak_x)^2]-2\gamma_{1,2}+\tfrac{1}{2}E^+(X_1),\\ B&=[\partial^2E^+(X_1)/\partial(ak_x)^2]-\tfrac{1}{2}\gamma_{0,1}+2\gamma_{1,1}+\tfrac{1}{2}E^+(X_1),\\ C&=-2[\partial E^+(X_1)/\partial(ak_x)]^2-4[\partial E^+(X_1)/\partial(ak_x)]\\ &\quad\times(\gamma_{1,1}+\gamma_{1,2})-8\gamma_{1,1}\gamma_{1,2}. \end{aligned} \tag{B8}$$

The fourth and final equation is obtained by rewriting Eq. (40) in terms of the variables of Eq. (B4) and is given by

$$[\mathfrak{L}_1b+\mathfrak{L}_2]=(d-2f)^2, \tag{B9}$$

in which

$$\mathfrak{L}_1=(\gamma_{0,1}-8\gamma_{1,1})$$

and

$$\mathfrak{L}_2=[E^+(X_1)-2\gamma_{1,2}-4L(\Gamma_{25'})]\mathfrak{L}_1. \tag{B10}$$

The simultaneous solution of Eqs. (B5)–(B7) and (B9) can be accomplished by eliminating the variables b, d, and f to obtain a quartic equation in the variable a. The roots of this quartic equation may be all real or complex in pairs. In practice, every real root is examined and most solutions are ruled out by the convergence requirement for the Fourier series (i.e., $|\gamma_{2,i}|\ll|\gamma_{1,i}|\ll|\gamma_{0,i}|$), so that the energy bands are adequately described by only a few terms in the Fourier series. For the set of experiments selected in this band-parameter determination, two roots are approximately equal and rapidly convergent, while the other two roots, which are poorly convergent are quite different from these and from each other. Because these poorly convergent solutions do not provide a good description of the dielectric constant, they are not considered as physically meaningful. Since the rapid convergent solutions can be made complex, in fact, complex conjugates of each other, by small changes of the band ordering, the experimental data is constrained and cannot be varied freely. Of these two solutions, the more rapidly converging one yields the better dielectric constant as well as energy bands which more closely resemble the calculated germanium bands. This most rapidly convergent solution of the four coupled equations yields values for a, b, d, and f, and in turn, the quantities $\gamma_{1,4}$, $\gamma_{2,4}$, $\gamma_{2,1}$, and $\gamma_{2,25}$ are evaluated for silicon.

APPENDIX C: SOLUTION OF COUPLED EQUATIONS IN GERMANIUM

For germanium, the seven variables $\gamma_{1,4}$, $\gamma_{2,1}$, $\gamma_{2,2}$, $\gamma_{2,3}$, $\gamma_{2,4}$, $\gamma_{2,5}$, and $\gamma_{2,6}$ are evaluated from solution of seven coupled equations. The seven pieces of experimental data that are introduced include the energy of the levels $E^+(L_1)=0.6643\pm0.0005$ eV,[59] and $E^+(X_1)=1.2\pm0.2$ eV, the effective mass of the conduction band $E(\Gamma_{2'})$ which is $m_{\Gamma_{2'}}{}^*/m_0=0.040\pm0.005$,[54,58] the longitudinal cyclotron effective mass of the conduction band $E^+(L_1)$, which is $m_l{}^*/m_0=1.58\pm0.02$,[14,15] and the three effective-mass quantities for the degenerate valence band $L(\Gamma_{25'})=-15.6\pm0.3$ eV, $M(\Gamma_{25'})=-2.21\pm0.18$ eV and $Q(\Gamma_{25'})=-0.07\pm0.84$ eV.[14,15,17,63] Since the value for $Q(\Gamma_{25'})$ is not well established from the cyclotron-resonance experiments, it can be estimated by Eq. (57) to be $Q(\Gamma_{25'})=-0.80\pm0.20$ eV. The energy $E^+(X_1)$ for germanium is estimated to be close to the value 1.2 eV, which is well established for silicon.

These seven experimental quantities determine the seven unknown band parameters listed above through a set of seven coupled equations. Six of the seven equations are easily written in explicit form, but the seventh, involving the longitudinal cyclotron effective mass of the conduction band is sufficiently complicated so that it is most conveniently solved by numerical procedures. For this reason, the six explicit equations are solved for six unknowns in terms of the seventh band parameter $\gamma_{2,2}$ and the experimentally measured quantities. There are several solutions for $\gamma_{2,2}$ that yield the experimental value for the longitudinal cyclotron mass and all of these solutions are examined. The solutions for $\gamma_{2,2}$ are readily found, since $\gamma_{2,2}$ is restricted to a small range of values.

An upper and lower bound on $\gamma_{2,2}$ is established by requiring that $\gamma_{1,4}$ and $\gamma_{2,6}$ be real, in accordance with the formulation of the effective-mass Hamiltonian in Sec. II. The first set of upper and lower bounds result from the expression for the energy of the $E^+(X_1)$ level which is given by Eqs. (17) and (18). This equation can be rewritten as

$$\gamma_{1,4}=\pm\tfrac{1}{4}\{[E^+(X_1)-\chi_{11}][E^+(X_1)-\chi_{22}]\}^{1/2}, \tag{C1}$$

and the reality condition on $\gamma_{1,4}$ implies that

$$[E^+(X_1)-\chi_{11}][E^+(X_1)-\chi_{22}]>0, \tag{C2}$$

in which

$$\begin{aligned} \chi_{11}&=\gamma_{0,1}-4\gamma_{1,1}-8\gamma_{2,1},\\ \chi_{22}&=\gamma_{0,2}-4\gamma_{1,2}-8\gamma_{2,2}+8\gamma_{2,5}. \end{aligned} \tag{C3}$$

The unknowns $\gamma_{2,1}$ and $\gamma_{2,5}$ can be eliminated from these equations by use of Eqs. (34b), (40), and (41). Substitution into Eq. (C2) results in the restriction on $\gamma_{2,2}$

$$(\alpha_0+24\gamma_{2,2})(\beta_0-24\gamma_{2,2})>0, \tag{C4}$$

where

$$\begin{aligned} \alpha_0=\gamma_{0,1}&-6\gamma_{1,1}-6\gamma_{1,2}+4[(\gamma_{1,3})^2/\gamma_{1,2}]+8M(\Gamma_{25'})\\ &+4L(\Gamma_{25'})+4[\partial^2E(\Gamma_{2'})/\partial(ak)^2]-E^+(X_1), \end{aligned} \tag{C5}$$

and

$$\beta_0=8\gamma_{1,2}-4[(\gamma_{1,3})^2/\gamma_{1,2}]-8M(\Gamma_{25'})-E^+(X_1). \tag{C6}$$

Upper and lower bounds on the value of $\gamma_{2,2}$ are also imposed by the reality requirement on $(\gamma_{1,4}+\gamma_{2,6})$, which follows from Eqs. (31) and (32a) for the energy

of the $E^+(L_1)$ level. These equations can be rewritten as

$$4\sqrt{3}\,|\gamma_{1,4}+\gamma_{2,6}| = \pm\{[2E^+(L_1)-A(L_1)-B(L_1)]^2 - [A(L_1)-B(L_1)]^2\}^{1/2}, \quad \text{(C7)}$$

in which

$$A(L_1)=\gamma_{0,1}-6\gamma_{1,1}-6\gamma_{2,1} \quad \text{(C8)}$$

and

$$B(L_1)=\gamma_{0,2}-2\gamma_{1,2}-4\gamma_{1,3}-6\gamma_{2,2}-4\gamma_{2,3}. \quad \text{(C9)}$$

The reality requirement for $(\gamma_{1,4}+\gamma_{2,6})$ leads to the restriction

$$[2E^+(L_1)-A(L_1)-B(L_1)]^2-[A(L_1)-B(L_1)]^2 = \beta_1{}^2-(\alpha_1+36\gamma_{2,2})^2>0. \quad \text{(C10)}$$

The unknowns $\gamma_{2,1}$ and $\gamma_{2,3}$ are eliminated from these equations by use of Eqs. (34), (40)–(42) to obtain

$$\alpha_1=\gamma_{0,1}-(15/2)\gamma_{1,1}-(27/2)\gamma_{1,2}+6\gamma_{1,3} +4[(\gamma_{1,3})^2/\gamma_{1,2}]+3L(\Gamma_{25'})+8M(\Gamma_{25'})+2Q(\Gamma_{25'}) +3[\partial^2E(\Gamma_{2'})/\partial(ak)^2], \quad \text{(C11)}$$

$$A(L_1)+B(L_1)=\alpha_1+18\gamma_{1,2}-12\gamma_{1,3}-2[(\gamma_{1,3})^2/\gamma_{1,2}] -4M(\Gamma_{25'})-4Q(\Gamma_{25'}), \quad \text{(C12)}$$

and

$$\beta_1=2E^+(L_1)-[A(L_1)+B(L_1)]. \quad \text{(C13)}$$

The range of allowed values of $\gamma_{2,2}$ is established by taking the most restrictive of the upper and lower bounds imposed by Eqs. (C4) and (C10).

With an arbitrary value for $\gamma_{2,2}$ but within the range of allowed values, the other six band parameters are evaluated according to the relations

$$\gamma_{2,1}=\tfrac{1}{4}\gamma_{1,1}+\tfrac{3}{4}\gamma_{1,2}-3\gamma_{2,2}-[(\gamma_{1,3})^2/2\gamma_{1,2}]-M(\Gamma_{25'}) -\tfrac{1}{2}L(\Gamma_{25'})-\tfrac{1}{2}[\partial^2E(\Gamma_{2'})/\partial(ak)^2] \quad \text{(C14)}$$

$$\gamma_{2,3}=3\gamma_{2,2}+\tfrac{1}{2}\gamma_{1,3}+[(\gamma_{1,3})^2/4\gamma_{1,2}]-\tfrac{3}{4}\gamma_{1,2}+\tfrac{1}{2}M(\Gamma_{25'}) +\tfrac{1}{2}Q(\Gamma_{25'}), \quad \text{(C15)}$$

$$\gamma_{2,5}=\tfrac{1}{2}\gamma_{1,2}-2\gamma_{2,2}-[(\gamma_{1,3})^2/2\gamma_{1,2}]-M(\Gamma_{25'}), \quad \text{(C16)}$$

$$\gamma_{1,4}=\pm\tfrac{1}{4}[\{\gamma_{0,1}-4\gamma_{1,1}-8\gamma_{2,1}-E^+(X_1)\} \times\{4\gamma_{1,2}-8\gamma_{2,2}+8\gamma_{2,5}-E^+(X_1)\}]^{1/2}, \quad \text{(C17)}$$

$$\gamma_{2,4}=\tfrac{1}{2}\gamma_{1,4}\pm\tfrac{1}{4}[\{L(\Gamma_{25'})-\tfrac{1}{2}\gamma_{1,2}+2\gamma_{2,2}-2\gamma_{2,5}\} \times\{8\gamma_{1,1}-\gamma_{0,1}\}]^{1/2}, \quad \text{(C18)}$$

$$\gamma_{2,6}=-\gamma_{1,4}\pm(1/4\sqrt{3})[\beta_1{}^2-(\alpha_1+36\gamma_{2,2})^2]^{1/2}. \quad \text{(C19)}$$

Arbitrary allowed values of $\gamma_{2,2}$ are scanned and from the resulting energy bands, this parameter is evaluated to obtain the experimental value for the longitudinal cyclotron effective mass.[14,15] In general, several such solutions are found and all mathematically valid solutions are examined. Some of these solutions are, in fact, equivalent and involve only the change in sign of a few band parameters. The most convergent solution also seems to yield the best dielectric constant, and for these two reasons is considered to be the most physical. This solution remains the most convergent under small changes in the band ordering. If, however, a major reordering of the energy bands is made, some other solution might become the most convergent and, therefore, provide the best description of the real solid.

PHYSICAL REVIEW VOLUME 160, NUMBER 3 15 AUGUST 1967

Conductance Anomalies due to Space-Charge-Induced Localized States

D. J. BENDANIEL AND C. B. DUKE
General Electric Research and Development Center, Schenectady, New York
(Received 4 November 1966; revised manuscript received 23 March 1967)

Space-charge-induced accumulation regions in semiconductors and semimetals can lead to localized, discretely spaced two-dimensional energy bands for which the existence criteria and the eigenvalue spectrum are derived. The contribution of these states to the conductance of a planar metal-oxide-semimetal (-semiconductor) tunnel junction exhibits structure associated with the critical points in the density of states for motion parallel to the junction. As an example, numerical results are given for Al-oxide-Bi junctions.

I. INTRODUCTION

THE existence of localized, quantized one-electron eigenstates in narrow accumulation or inversion layers at semiconductor surfaces has been conjectured for at least ten years.[1–3] However, only surface transport measurements[4–8] have given evidence for the existence of these states, and the interpretation of those experiments is qualitative, owing to the lack of a microscopic quantum theory of surface transport.[3] Optical

[1] J. R. Schrieffer, *Semiconductor Surface Physics*, edited by R. H. Kingston (University of Pennsylvania Press, Philadelphia, Pennsylvania, 1957), p. 68.
[2] J. F. Dewald, Ann. N. Y. Acad. Sci. **101**, 872 (1963).
[3] R. F. Greene, Surface Sci. **2**. 101 (1964).
[4] P. Handler and S. Eisenhouer, Surface Sci. **2**, 64 (1964).
[5] N. St. J. Murphy, Surface Sci. **2**, 86 (1964).
[6] F. Proix and P. Handler, Surface Sci. **5**, 81 (1966).
[7] F. F. Fang and W. E. Howard, Phys. Rev. Letters **16**, 797 (1966).
[8] A. B. Fowler, F. F. Fang, W. E. Howard, and P. J. Stiles, Phys. Rev. Letters **16**, 901 (1966).